Article

Classification of Dynamical Diffusion States in Single Molecule Tracking Microscopy

Peter J. Bosch,[1] Johannes S. Kanger,[2] and Vinod Subramaniam[1,2,*]
[1]Nanobiophysics, MESA+ Institute for Nanotechnology, University of Twente, The Netherlands; and [2]MIRA Institute for Biomedical Technology and Technical Medicine, University of Twente, The Netherlands

ABSTRACT Single molecule tracking of membrane proteins by fluorescence microscopy is a promising method to investigate dynamic processes in live cells. Translating the trajectories of proteins to biological implications, such as protein interactions, requires the classification of protein motion within the trajectories. Spatial information of protein motion may reveal where the protein interacts with cellular structures, because binding of proteins to such structures often alters their diffusion speed. For dynamic diffusion systems, we provide an analytical framework to determine in which diffusion state a molecule is residing during the course of its trajectory. We compare different methods for the quantification of motion to utilize this framework for the classification of two diffusion states (two populations with different diffusion speed). We found that a gyration quantification method and a Bayesian statistics-based method are the most accurate in diffusion-state classification for realistic experimentally obtained datasets, of which the gyration method is much less computationally demanding. After classification of the diffusion, the lifetime of the states can be determined, and images of the diffusion states can be reconstructed at high resolution. Simulations validate these applications. We apply the classification and its applications to experimental data to demonstrate the potential of this approach to obtain further insights into the dynamics of cell membrane proteins.

INTRODUCTION

It remains an elusive dream to be able to follow a protein and its interactions as the protein travels through the cell during its lifespan. Nevertheless, single molecule tracking by fluorescence microscopy allows one to follow a protein in a living cell at high resolution for a short period of time and to record its trajectory (1–6). Tracking of proteins in live cells is a unique approach to obtain details on dynamical protein association and dissociation kinetics in a spatiotemporal manner, and complements other fluorescence microscopy techniques (7–9). Single molecule tracking techniques have given us valuable insight into the dynamics and biological functions of proteins (6,10–12) and the organization of the plasma membrane (13–16). Despite methodological advances and the insight obtained by contemporary analysis methods, there remains a need to further develop analysis tools that can translate experimental data into biological insights. For example, spatiotemporal information on the diffusion of membrane proteins would contribute to a biophysical understanding of the organization of these protein complexes.

Trajectories of proteins obtained by tracking techniques contain information about the interaction and functional states of the protein. For example, the phosphorylation state of many membrane-bound tyrosine kinase receptors is related to the formation of dimers or higher-order aggregates (17,18). Clearly, proteins associated with these aggregates are expected to show lower mobility than free monomeric receptor molecules, which is reflected in their trajectories. Additionally, proteins often transiently interact with other molecules in nanoscale compartmentalization structures in the plasma membrane or with cytoskeletal structures, both resulting in transient slowed diffusion or confinement (4–6,19–23). Not only do interactions with molecules alter protein mobility, but the mobility of a protein also affects the possibility of interactions with other molecules (24–26). A detailed knowledge of the interactions of proteins and their dynamics is therefore important to understand the underlying signal transduction processes and to model the cellular signal regulatory system (24–28).

Translating the trajectories of proteins to biological events, such as protein interactions, requires the classification of protein motion within the trajectories. Protein species transiently exhibit different types of motion. The motion of membrane proteins can often be described by two dynamic populations of pure Brownian diffusion (6,19,23), which we refer to as the diffusion states (Fig. 1 *A*). It is, however, nontrivial to accurately determine in which diffusion state the protein is residing during the measured trajectory. Several issues hamper faultless state classification. Proteins exhibiting different diffusion states often have overlapping distributions of step sizes (Fig. 1 *B*). Furthermore, the localization of proteins has a limited accuracy, and the switching

Submitted February 4, 2014, and accepted for publication May 29, 2014.

*Correspondence: subramaniam@amolf.nl

V. Subramaniam's present address is FOM Institute AMOLF, Science Park 104, 1098 XG Amsterdam, The Netherlands.

Editor: Paul Wiseman.

0006-3495/14/08/0588/11 $2.00

http://dx.doi.org/10.1016/j.bpj.2014.05.049

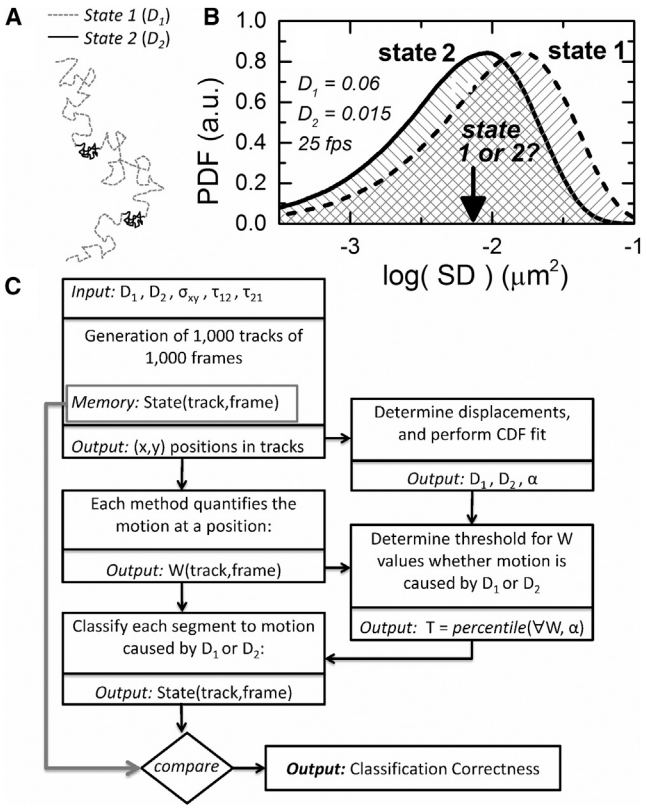

FIGURE 1 Proposed framework for state classification and problem statement. (*A*) Schematic to illustrate a typical trajectory of a single protein on a plasma cell membrane, displaying switching behavior between two states with different diffusion coefficients. (*B*) Distributions of observed squared displacements (*SD*) resulting from different diffusion coefficients show large overlap. A measured step-size value (an example is indicated with an *arrow*) cannot be classified with high certainty to unambiguously originate from a particular state, which demonstrates one of the problems to be solved for diffusion state classification. To compose this histogram, a localization inaccuracy σ_{xy} of 40 nm was added to the positions in the simulations. (*C*) Scheme of the methodology followed to test the various classification methods on correctness of state classification. After generation of simulated trajectories with dynamic-state allocation, we determine the diffusion constants (D_1 and D_2) and the fraction (α) of the fast state from all displacements using a CDF fit. The track is divided into segments of a certain window length (N), and for each segment the tested quantification methods provide a value W using only the positions in that segment. For each segment the motion is classified as fast or slow diffusion. The threshold (T) for classification is determined from all values W and the fraction α. The center position of the segment is classified as slow diffusion when W is smaller than the threshold T, and as fast diffusion otherwise. The found state is compared with the actual (remembered) state to yield the classification correctness. The same scheme is followed for the diffusion state classification of experimental data. Although the correctness clearly cannot be determined in that case, an estimation of the correctness can be determined by performing simulations at the parameters found by the CDF fit.

between the diffusion states is a stochastic process. Diffusion-state classification methods are needed to determine when, and in what regions, the protein exhibited distinct diffusion behavior. These regions might point toward a role of certain cellular structures in the function of the studied protein species. In addition, the lifetimes of these diffusion states (the inverse kinetic rate) can be directly derived from the diffusion state durations, and are useful parameters to comprehend the role of the studied protein in complexes associated with cellular regulatory systems. The combined insight may eventually reveal the spatiotemporal design principles of cell decision-making (27).

A widely used analysis method for single molecule tracking data considers complete trajectories using mean-squared displacement (MSD) curves (3,29–32). For homogenous motion, the shape of the MSD curve contains information about the nature of the diffusion, e.g., pure, confined, or hop diffusion (3,13,33,34). Because the MSD curve is composed of averages of all distances, transient diffusion states cannot be resolved by these full-trajectory MSD analyses (see Fig. S1 in the Supporting Material). When it was realized that protein motion is not homogeneous, but shows transient effects (1,4,10,22,35), local methods were developed that considered subtrajectories (segments) of a trajectory (4,34,36,37). These methods are hampered, however, by the limited number of positions within one segment to obtain accurate diffusion coefficients or confinement strengths. An alternative Monte Carlo-based method (38) is particularly useful to find the kinetic rates between well-differentiated diffusion populations. This method finds diffusion coefficients, their fractions, and the switching rates for the whole set of trajectories, but does not spatially resolve the states. Therefore, we propose what we believe to be a new approach that uses a global method (analyzing all trajectories obtained) to determine the different diffusion states of the protein studied, whereas local methods are used to classify short segments of a trajectory to one of the diffusion states found. We compare several local methods to classify parts of trajectories (segments) to a diffusion state.

Proposed scheme for diffusion state classification

For pure diffusion systems, the multiple diffusion states can be accurately determined using a fit of the cumulative distribution function (CDF) of the squared displacements (20). In this article, we assume that the motion of membrane proteins can be described by two states of Brownian diffusion, termed the "fast" and the "slow" population. Whether this assumption is correct can be checked beforehand by looking at the residuals of a fit of the CDF of step sizes in two-population diffusion (detailed later). After obtaining accurate diffusion parameters by this fit, local methods are used only to classify short segments of a trajectory to one of the diffusion states found. Existing local diffusion or confinement detection methods (34,36,37) can be expanded to yield a local quantification measure that can be used for classification. Subsequently, the classification to a diffusion state is based on a threshold for the quantification measures.

This threshold is objectively set using the parameters describing the diffusion states (determined by the fit), and the threshold is therefore based on the experimental data. Thereby, we eliminate the subjective manual thresholding of earlier confinement methods to detect transitions between motion states. The need for manual thresholding was earlier mentioned as a disadvantage of using window (segments)-based methods (39).

We emphasize that there is no need to determine local diffusion values of segments, because the CDF fit has already accurately provided the diffusion values present within the trajectories. The segments only need to be classified to one of the diffusion states. The length of the segments should be carefully chosen such that the corresponding duration is shorter than the typical switching time between states, whereas the duration must be long enough to obtain an accurate measure for the classification. We test different local methods and the influence of different segment lengths for diffusion classification using two-state Brownian dynamics simulations (Fig. 1 *C*), and compare this approach to a recently developed Bayesian method (40).

Existing motion classification schemes

Several schemes have been proposed to differentiate between the supposed motion types of single proteins found in (sub)trajectories, such as directed, confined, and normal diffusion (33,39,41,42). Three of these schemes consider classification of pure diffusion states (40,43,44). Two of these schemes were based on maximum likelihood estimation (MLE). The scheme devised by Ott et al. (44) employs an MLE approach to classify between diffusive states (also included in our comparison), and uses hidden Markov models to find the diffusion coefficients of these states. The other scheme relies on a large number of localizations and a prior defined number of diffusion-state switching occurrences (43). With contemporary fluorescence microscopy techniques, it is still impossible to accurately localize many positions to find the actual state before the protein switches between states. Furthermore, the amount of diffusion-state switching occurrences is not known beforehand, because this switching is a stochastic process. In 2004, another scheme was proposed that used Bayesian statistics (45) to discriminate between slow and fast Brownian motion in a spatiotemporal fashion without prior knowledge (40). This scheme combines information from thousands of short trajectories to identify the number of diffusive states and the state transition rates, and is included in our comparison.

The classification of confined motion, i.e., motion hindered by transient confinement zones, has been discussed elsewhere (3,20,22,38,39). We emphasize that our approach is not in contrast to the idea of transient confinement zones. In fact, whether the slow diffusion state originates from pure Brownian motion, a transient confinement, or an immobilization of the protein, cannot be revealed from the limited number of typically acquired positions, and requires other experimental and analytical methods. Although the transient confinement and slowed diffusion are closely related, confinement is actually defined as pure diffusive motion restricted by boundaries that cannot be crossed. The confinement area should be of reasonable size such that normal diffusion within this area can still occur. There is no consensus yet on the exact type of motion proteins exhibit.

MATERIALS AND METHODS

Classification scheme

We provide an overview of our approach to test classification of segments to dynamic two-population diffusion states (Fig. 1 *C*), followed by a more detailed description of the individual steps. To begin, the two diffusion coefficients and their fractional contribution to the trajectories are determined using a CDF fit of the squared displacements (20). Next, we use one of the different local quantification methods, listed in Quantification Measures in the Supporting Material, which assigns a value to each position in the trajectory. All these methods yield a higher value for a higher diffusion speed. Subsequently, thresholding of these values for the classification is done by taking the αth percentile value of all values found (with α the percentage of step sizes fitted to the first population). For example, when the fraction size of fast diffusion is 0.30, we set the threshold value such that 30% of the values are higher than the threshold value. By taking this threshold, we perform the classification objectively, because the fraction percentage is already accurately determined beforehand from the experimental data itself. To compare the different detection methods in this framework, we tested them using simulated trajectories, where we know the actual diffusion state at each position. The final step in testing the framework is a one-to-one comparison of the found state to the actual (simulated) diffusion state, yielding the classification correctness. We define the classification correctness as the percentage of positions that are correctly classified divided by the total number of classified positions. The state lifetimes τ_1 and τ_2 found by the analysis are compared with the actual lifetimes for the most promising method.

Generation of synthetic trajectories

Two-population diffusion trajectories were generated using MATLAB (The MathWorks, Natick, MA) with the GPUMAT toolbox (8). Each set contained 1000 trajectories composed of 1000 frames (positions) in two dimensions with Brownian diffusion steps in between points. The molecule is allowed to change between diffusion states within a trajectory. In more detail, the positions are given by

$$x_{i+1} = x_i + R \cdot \sqrt{2D_j \Delta t}, \quad (1)$$

$$y_{i+1} = y_i + R \cdot \sqrt{2D_j \Delta t}, \quad (2)$$

where i is the frame number, R is a random number from a standard normal distribution, D_j is the diffusion coefficient of the diffusion state j, and Δt is the time between frames ($\Delta t = 40$ ms unless otherwise stated). The dynamical switching behavior between the two diffusion states (e.g., $j = 1$, also called fast, and $j = 2$, also called slow) is provided by generating subsequent state durations. The duration of the state is determined by taking a random number from an exponential distribution (a Poisson process) with a given characteristic time τ_1 and τ_2. Diffusion states of all steps in the set are stored, to be able to verify the classification method. Each position

(x_i, y_i) is given a localization inaccuracy error by adding a random number from a normally distributed pool with standard deviation σ_{xy} in each dimension. The localization error in the x-plane σ_x is equal to the error in the y-plane σ_y, therefore $\sigma_{xy} = \sigma_x = \sigma_y$.

Cumulative distribution function of squared displacements

To find the diffusion constants D_1 and D_2 and the fraction α of the first population, we calculate the cumulative distribution function of squared displacements for the complete set of trajectories (20). Using the complete distribution yields insights into the behavior of the entire population of single molecules, without ensemble averaging effects. As long as there is a large dataset of displacements to build a reliable CDF, it is a straightforward and reliable method to find the global diffusion coefficients and their fractions. For the two-dimensional case, the CDF for the squared displacements $(\Delta R)^2$, for a time lag $\tau = n \cdot \Delta t$, for two diffusion components is given by

$$\mathrm{CDF}\left(\Delta R^2(\tau)\right) = 1 - \alpha \cdot \exp\left(-\frac{(\Delta R)^2}{4\ D_1\tau + 2\left(\sigma_x^2 + \sigma_y^2\right)}\right) - (1-\alpha)\cdot \exp\left(-\frac{(\Delta R)^2}{4\ D_2\tau + 2\left(\sigma_x^2 + \sigma_y^2\right)}\right), \tag{3}$$

where α is the fraction corresponding to the motion with diffusion coefficient D_1. To deal with the localization inaccuracy in the exponent, we determine D_1, D_2, and α for the time lags corresponding to one and two frames, and fit the exponential terms:

$$\mathrm{CDF}\left(\Delta R^2(1)\right) = 1 - \alpha_{\tau=1} \cdot \exp\left(-\frac{(\Delta R)^2}{4\ \widehat{D}_{1,\tau=1}}\right) - (1-\alpha_{\tau=1})\cdot \exp\left(-\frac{(\Delta R)^2}{4\ \widehat{D}_{2,\tau=1}}\right), \tag{4}$$

$$\mathrm{CDF}\left(\Delta R^2(2)\right) = 1 - \alpha_{\tau=2} \cdot \exp\left(-\frac{(\Delta R)^2}{4\cdot 2\ \widehat{D}_{1,\tau=2}}\right) - (1-\alpha_{\tau=2})\cdot \exp\left(-\frac{(\Delta R)^2}{4\cdot 2\ \widehat{D}_{2,\tau=2}}\right), \tag{5}$$

which yield the uncorrected diffusion coefficients for each time lag, for example,

$$\widehat{D}_{1,\tau=1} = D_{1,\tau=1} + \sigma_{xy}^2,$$

because ${\sigma_x}^2 + {\sigma_y}^2 = 2{\sigma_{xy}}^2$, and similarly

$$2\ \widehat{D}_{1,\tau=2} = 2\cdot D_{1,\tau=2} + \sigma_{xy}^2.$$

Now the estimated diffusion coefficient for the first (and similarly for the second) population corrected for the localization error is

$$\begin{aligned} D_1 &= 2\widehat{D}_{1,\tau=2} - \widehat{D}_{1,\tau=1} \\ &= \left(2D_{1,\tau=2} + \sigma_{xy}^2\right) - \left(D_{1,\tau=1} + \sigma_{xy}^2\right) \\ &= 2D_{1,\tau=2} - D_{1,\tau=1}. \end{aligned} \tag{6}$$

For the fraction α we take the average of the values $\alpha_{\tau=1}$ and $\alpha_{\tau=2}$. In the simulations, these two values did not differ by more than a few percent. We have used linear least squares to fit the CDF to the data. Fig. S11 shows an example of a CDF fit for motion with two clearly separated diffusion populations.

Quantification measures

The next step is to quantify the motion of a molecule for each frame in its trajectory. To this end, the trajectories are split in small segments, containing a total number of N subsequent positions (the segment length), and these segments are given a value W by one of the tested quantification measures. Many methods could serve as a measure for slow or fast diffusion. This measure can be, but is not limited to, an estimated diffusion coefficient or confinement index. We have tested the following methods: windowed MSD (34), relative confinement (35,36), the gyration radius (37), and MLE. Besides these windowed measures, we also tested a Bayesian statistics approach (40) using software made available by these authors. A detailed discussion of the measures used can be found in Quantification Measures in the Supporting Material.

State classification

When the motion within a segment is quantified, it can be classified as State 1 (corresponding to fast diffusion with coefficient D_1) or as State 2 (corresponding to slow diffusion with coefficient D_2). We allocate the classification of the segment to the center position of that segment, so that a state duration can still be shorter than the segment length. For the MLE, the classification is performed intrinsically. For the relative confinement and gyration radius methods, the classification is provided by comparing the value W to a threshold value T. A segment is classified as State 1 if W is larger than a threshold value T, and as State 2 otherwise. The threshold value T is determined by taking all found values W, and calculating the αth percentile of these values (with α the percentage of step sizes fitted to the first population). Hence, the already known fraction of the diffusion population is used to define the threshold value for the measure to perform the classification.

In the case of the windowed MSD, we slightly altered the way to determine the threshold T, due to reasons described in the Results. We used a likelihood approach to calculate the chance that a single value W (calculated for a segment) originates from diffusion with D_1 or originates from diffusion with D_2. In more detail, a probability density function (PDF) of W is composed for each diffusion constant given the values of the diffusion coefficients D_1 and D_2. Examples of such PDFs are shown in Fig. S12 *A*. The threshold value T is chosen as that value of W where the PDF of W from D_1 intersects the PDF of W from D_2 (such that $L_1(T) = L_2(T)$). In this way, the segment is classified to the most likely state.

The PDF of W for the windowed MSD method for a given diffusion coefficient is calculated as follows: Using a one-population Brownian simulation, a trajectory (containing 10^6 positions) is calculated. From this, we calculated the values W for all segments in the trajectory. Next, the PDF of the found values W is composed. This procedure is performed for both D_1 and D_2. Finally, the intersection of these two PDFs is determined.

Visualization

After the state classification has been performed, either in simulations or in experimental data, the information obtained can be used for subsequent

analysis such as visualization. All the positions of all the molecules in one video recording are used to reconstruct an image, such that one can visualize the areas where the molecules have traveled. Each individual position (localization) is represented by a color-coded dot. The color of the dot depends on the state found at that position and time: red for the slow state, and green for the fast state. This results in diffusion-state images at high resolution showing the areas of slow and fast diffusion. We removed immobile trajectories because these were typically found on the glass substrate and not in cells. The filter for immobile trajectories was based on the gyration method applied on a complete trajectory, with the threshold for the reached area defined by a gyration radius of 40 nm, as this corresponded to the apparent area traveled by an immobile molecule due to the localization accuracy. This means that only those molecules are displayed that exhibit motion at least once.

Live cell experiments

See Live Cell Experiments Methodology in the Supporting Material.

RESULTS

Performance of different quantification measures

We validated our approach by simulating the extreme case of well-separated diffusion constants with $D_1 = 40 \times D_2$ and long-state durations. We obtained a correctness of >95% for windowed MSD, and >99% for the other methods, as expected for clearly distinct motion. Next, we tested the different quantification measure methods for diffusion classification, and studied the influence of different segment lengths therein. Therefore, we simulated (at 25 fps) four cases with two diffusion states with different state lifetimes and localization accuracy. The cases were chosen to provide a challenging and realistic situation for discrimination of the two diffusion constants from experimentally obtained single molecule trajectories.

The diffusion constants were chosen to reflect relatively slow membrane receptors (unpublished observations): $D_1 = 0.06\ \mu m^2/s$, and $D_2 = 0.015\ \mu m^2/s$. (For other ratios of diffusion coefficients, see Fig. S4.) We chose our switching settings close to the values found for the epidermal growth factor (EGF) receptor (4): $\tau = 300$–900 ms. The localization accuracy depends on the number of photons recorded from a molecule per frame. The chosen localization accuracies are typical values observed for quantum dot labels ($\sigma_{xy} = 20$ nm) or fluorescent protein labels ($\sigma_{xy} = 40$ nm), whereas organic dyes will often be somewhere in between these values. The accuracy does not only depend on the number of photons acquired for localization, but also on the labeling strategy. For instance, antibodies are large macromolecules and their flexibility leads to a lower localization accuracy.

Fig. 2 shows the performance of diffusion-state classification for different quantification measures of local diffusion together with the influence of the segment length chosen. For the windowed MSD method, we display the correctness when using the first three points of the MSD curve in the fit, because this gave the best correctness in all the simulation

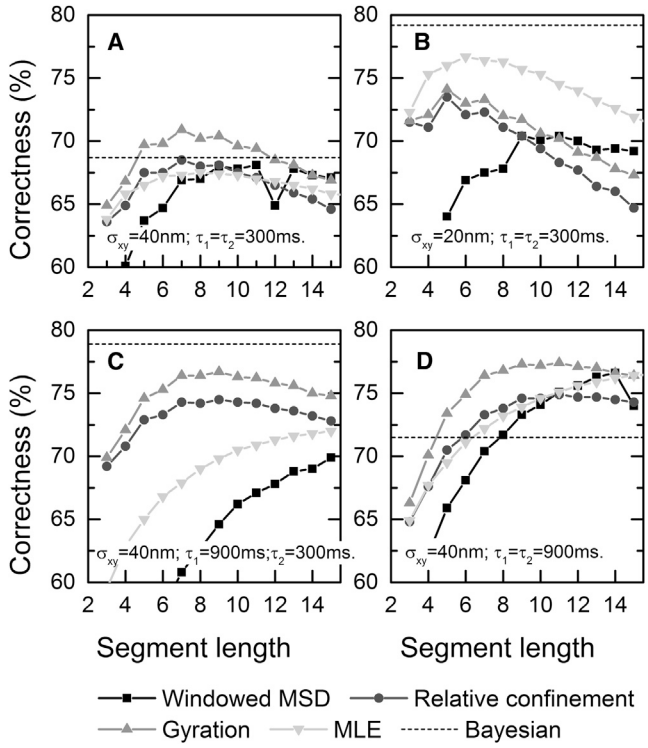

FIGURE 2 Correctness of the two-population classification by different quantification measures for different simulated cases (*A–D* in the corresponding panels). The correctness of the different quantification measures is plotted against the segment lengths used in the classification. The Bayesian method does not use segments, and its result is shown (*dashed line*). In all simulation cases $D_1 = 0.06\ \mu m^2/s$ and $D_2 = 0.015\ \mu m^2/s$. (*A*) Simulation case A has a localization inaccuracy σ_{xy} of 40 nm and short state lifetimes (τ_1 and τ_2). (*B*) This simulation case differs from case A only by a lowered localization inaccuracy σ_{xy}. (*C*) This simulation case differs from case A only by having a longer fast-state lifetime τ_1. (*D*) This simulation case also has a longer slow-state lifetime τ_2.

cases. For the first simulation (case A), we chose the localization accuracy $\sigma_{xy} = 40$ nm and the state lifetimes were both set to 300 ms. To study the influence of the localization accuracy σ_{xy} alone, in simulation case B this parameter was lowered to 20 nm. In simulation cases C and D, only the switching behavior was altered compared to case A to be able to test the influence of the state lifetimes. When the two lifetimes are not equal (case C), this clearly changes the diffusion fractions, such that there are an unequal number of molecules in each state on average. The two diffusion coefficients and their fractions were not assumed to be known beforehand, analogous to experimental data. These state parameters are found for each simulation by a fit to the CDF of squared displacements. The results show that an optimal choice of the segment length is needed to yield the best classification correctness. The optimal segment length depends to a large extent on the state lifetimes and also on the particular quantification measure used in the state classification.

We find that the non-diffusion-based gyration evolution method is the most accurate measure for diffusion-state

classification in the simulation cases, with localization accuracy of 40 nm (cases A, C, and D). In these cases, for equally sized diffusion populations (cases A and D), the gyration-based classification scores better than classification using any other method. When the diffusion populations are not equally sized (case C), the gyration-based classification scores almost as well as the computationally much more expensive Bayesian method. In simulation case B with a localization accuracy of 20 nm, the Bayesian method and MLE-based classification score better than the other methods. This trend continues when there is no localization inaccuracy; simulations for this case showed the MLE method then scores 81% correct compared to 74% for the gyration-based classification. In practice, however, the localization will rarely be better than 20 nm, due to the limited number of photons and biochemistry labeling-related issues. In the case of slow-state switching behavior (case D), the gyration-based classification at these state-switching rates is already close to its best possible performance with these diffusion coefficients and localization inaccuracy; increasing the average state duration to infinity only resulted in 3% improvement in correctness. The classification correctness for the windowed MSD achieved when another number of points in the MSD curve is taken to perform the fit can be found in Fig. S2. The classification correctness when we set a minimum state duration for a number of frames can be found in Fig. S3.

After classification of the diffusion inside trajectories, the lifetime of the states can be determined by composing a histogram of state durations and fitting the lifetime. We determined the distribution of the slow- and the fast-state lifetimes found by the gyration-based classification in trajectories of simulation case A (see Fig. S5). We found that the state lifetimes fitted are shorter than the actual (simulated) lifetimes, especially for longer state lifetimes. Additional simulations showed that a trend of changing the state lifetimes in the simulation is reflected in the lifetimes found, although larger lifetimes (as in case D) are significantly underestimated, especially when the correctness is $<85\%$.

Although the correctness percentages provide a measure of the classification performance, the exact number might not give a feeling for how useful such a classification is. We will return to this point in the section on identifying the zones of slow diffusion. Clearly the percentage must be $>50\%$ to have any relevance, because this percentage would also be obtained by a completely random state allocation.

Optimized threshold

The windowed MSD, relative confinement, and gyration measures use a threshold for classification. We noticed that for the windowed MSD, the classification correctness was not around its maximum with the threshold at the αth percentile, especially for unequally sized diffusion populations (Fig. 3 *A*). In the case of simulation case C (i.e., with unequally sized diffusion populations), the best result when using the windowed MSD as the quantification measure would be to classify every position as fast diffusion, and thereby scoring ~75% correct (i.e., the fast fraction size). However, such classifications would not provide any information. The other methods score the same correctness at the 100th percentile threshold by definition, but these methods score a higher correctness with a threshold at the αth percentile. For the windowed MSD method, we therefore used another threshold. We instead compared the likelihoods that a value W for a segment originates from diffusion with diffusion coefficient D_1 or from diffusion with diffusion coefficient D_2. In other words, the threshold was set at the intersection of the probability density functions of the values obtained with the windowed MSD for diffusion

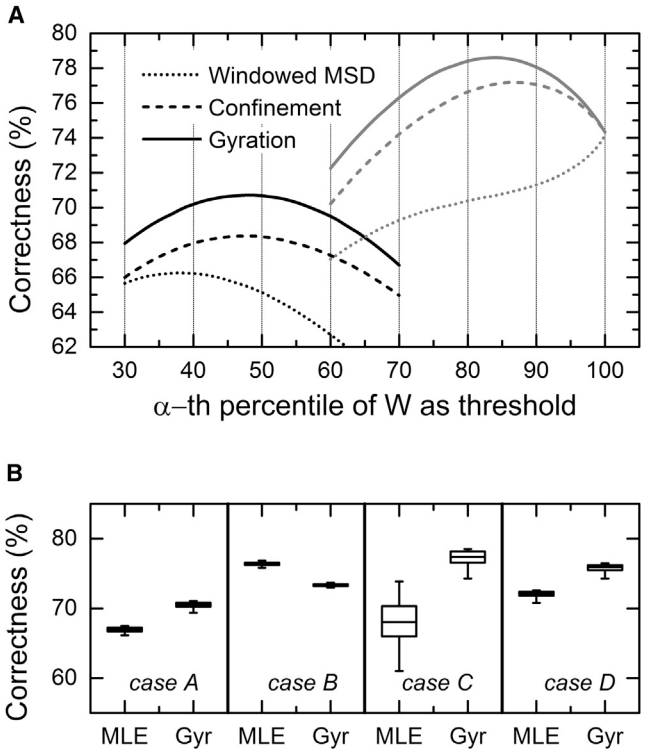

FIGURE 3 (*A*) The correctness dependence on the choice of the state classification threshold for simulation case A (*left curves*) and case C (*right curves*). The threshold varied with the αth percentile value of calculated quantification-measure values W. In these simulation cases, the fraction size for fast diffusion $\alpha = 0.5$ and $\alpha = 0.75$ (cases A and C, respectively), and the classification, was performed with a segment length of seven frames. The windowed MSD method does not yield optimal correctness with a threshold using the αth percentile, yet the optimal threshold does not provide any information either. Therefore the threshold selection for this method was altered to using the likelihood that the found value for a segment corresponds to either of the two diffusion states. (*B*) Robustness of the MLE and gyration-based classification. When simulations with 100 trajectories and 1000 frames are repeated 100 times, variations can come from the accuracy of the CDF fit. (*Box plot*) Resulting distribution (5, 25, 50, 75, 95%) of the obtained classification correctness using MLE and the gyration (*Gyr*) method for all simulation cases (*A–D*, *left* to *right*) due to this effect.

from each diffusion state separately (detailed in Materials and Methods). We verified that the windowed MSD using likelihoods for state classification indeed performed with a higher correctness compared to when window MSD values are compared to a threshold using the αth percentile. Likelihood methods do not regard the fraction size α to determine the most likely state for a segment, therefore the MLE and the Bayesian methods are not included in Fig. 3 *A*.

Classification robustness

The values for the classification performance in Fig. 2 and Fig. 3 *A* are average values that are obtained for many classifications. Because one simulation entailed 1000 trajectories of 1000 frames, the statistical noise averaged out between simulations with the same diffusion parameters. However, analyzing the results of one simulation is not sufficient to predict the robustness of the method, because the robustness in the correctness also depends on other aspects of the classification framework. For example, the correctness depends in large extent on the fitted diffusion constants and fractions obtained from the CDF fit. Therefore, we tested whether small perturbations in the CDF fit influenced the obtained correctness for the MLE and gyration method. We used a segment length of seven frames to classify 100 simulations to obtain the distribution of the correctness. In each simulation we used the simulation settings of case A, except for the number of trajectories in the simulations, which was lowered to 100 trajectories (a realistic number of molecules in a tracking experiment). In this way, fewer displacements are available for the CDF fit, and therefore the fitted values have a larger spread in subsequent simulations. The resulting correctness distributions (Fig. 3 *B*) shows that neither of the two methods is influenced dramatically by slightly perturbed CDF fits, except for the case where both fractions are not equally distributed (case C). The spread, in that case, is especially large in the MLE method.

Identifying the zones of slow diffusion

After state classification of the diffusion, super-resolution-like images of the diffusion states can be reconstructed. When the distribution of slow diffusion zones is not randomly distributed, the proposed approach for diffusion-state classification should be able to detect these zones. To validate this application, we performed simulations of 200 trajectories where the diffusion state was spatially defined. The regions with slow diffusion were defined as 1 pixel wide (corresponding to 120 nm), and were separated by 5 pixels. The separations were the regions of fast diffusion. The diffusion value in the fast region was chosen $D_1 = 0.10\ \mu m^2/s$, and in the slow regions it was chosen $D_2 = 0.01\ \mu m^2/s$, with the localization accuracy $\sigma_{xy} = 20$ nm. These settings were chosen to represent a typical membrane protein imaged utilizing bright fluorophores. The resulting state lifetimes were ~300 ms. We performed the diffusion-state classification using the gyration-quantification measure with a segment length of four frames (Fig. 4 and see Movie S1 in the Supporting Material). Simulations with the diffusion-state parameters mentioned showed that this is the optimal segment length. The correctness of gyration-based classification was 85%. The figure shows that the performance is more than adequate to visualize the spatial diffusion-state organization described. The actual states of the simulation and the same reconstruction image using MLE-based classification are shown in Fig. S7. For comparison, when the motion and the state switching is completely random, such as in simulation case A, the reconstruction map also shows apparent zones (see Fig. S6). However, these zones are only caused by the randomness of Brownian movement.

Example of classification applied to EGF receptor

The advantage of spatiotemporal-resolved state classification is the possibility to observe where the molecules have traveled in which diffusion state. Reconstructed videos may also reveal whether multiple diffusion populations are originating from a pool of molecules exhibiting either diffusion state, or a pool of molecules transiently making transitions between the states. The lifetimes of the states can be determined as well from the histogram of state durations.

To demonstrate the potential of the application of diffusion-state classification, we performed a gyration-based classification on experimental single molecule tracking data. We recorded fluorescence images of fluorescently labeled EGF receptor in MCF7 cells by utilizing SNAP-tag (see Movie S2). In this video recording we detected, on average, 210 fluorescent molecules per frame (see Fig. S8 *D*). The localization accuracy in our video is close to 40 nm. The diffusion constants D_1 and D_2 and the fraction size α of the fast state from all displacements are determined using a fit to the

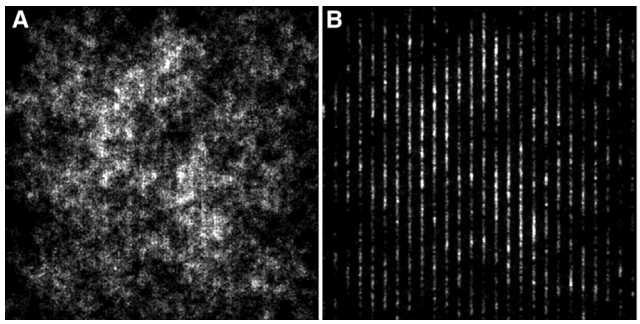

FIGURE 4 Diffusion states classified by the gyration method, visualized at high-resolution, with images displaying the regions in the fast state (*A*) and slow state (*B*). The simulation was designed with spatially defined zones (*vertical lines*) for diffusion states. Here the slow-state regions were 120-nm wide and are separated by 600-nm-wide fast-state regions. The regions of the slow diffusion state are suitably classified and clearly visible. The dimension of the image is 15 × 15 μm, and the image is reconstructed at a resolution of 30 nm/pixel.

CDF of squared displacements (see Fig. S8). We obtained $D_1 = 0.112 \pm 0.001$ $\mu m^2/s$, and $D_2 = 0.008 \pm 0.001$ $\mu m^2/s$ with $\alpha = 0.69 \pm 0.03$ (the given errors are 5–95% confidence intervals of the fit). Intercellular differences are larger than the errors of fitting the CDF. We used a segment length of seven frames, which performs best according to simulations for the given diffusion parameters (classification correctness of 86%). State lifetimes (or kinetic rates, the inverse lifetime) were obtained by combining the state durations from five recordings of EGF receptor (unliganded) to get enough statistics (see Fig. S9).

After diffusion-state classification, we reconstructed the diffusion-state video (see Movie S3) and diffusion-state images at high resolution (Fig. 5 and see Fig. S10). In these images, we clearly see distinct zones of slowed diffusion. Furthermore, we see cellular structures such as filopodia at the boundaries of the cell, and possibly collapsed filopodial structures on the lower membrane. The presence of EGF receptor in filopodia was expected, because EGF receptor undergoes retrograde transport in filopodia (46,47).

DISCUSSION

The optimal segment length

The optimal segment length correlated to the state lifetime in our simulations. For example, the optimal seven frames in simulation cases A and B corresponds to the average state lifetime of 300 ms (7.5 frames), and when the state lifetimes increase (simulation cases C and D), the optimal segment length also increases. The optimal segment length also varies for the different quantification measures, especially when the state lifetimes increase (simulation cases C and D). Because the state lifetimes are not known before the classification, it would be preferable when the results do not vary much for different segment lengths. We can see that the gyration method with a segment length of seven frames scores near optimal in almost all the cases simulated. Therefore, a good strategy would be to perform the classification first with the gyration method and a segment length of 5–7 frames. This might provide a good first classification with an adequate correctness. Later, the classification may be repeated with a different segment length more suitable to the state lifetimes found to obtain an optimized classification or a verification of the reconstructed diffusion-state images.

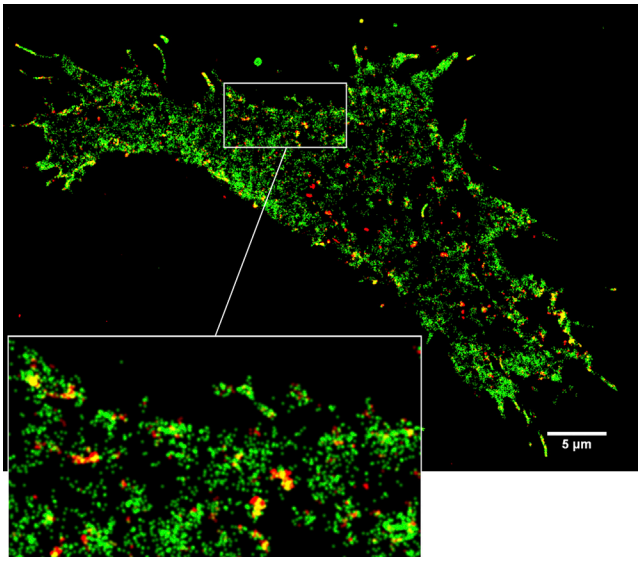

FIGURE 5 The spatial distribution of the diffusion states exhibited by EGF receptors in an MCF7 cell. The reconstructed image shows the areas where receptors were classified in the fast diffusion state (*green*), and areas where receptors were classified in the slow diffusion state (*red*). For a region at the periphery of the cell, a zoomed image (*inset*) shows clear regions of slow diffusion. The image also shows that the receptor is associated with certain cellular structures such as filopodia. The classification is performed using the gyration method with a segment length of seven frames. The resolution of the reconstructed image is 30 nm/pixel. To see this figure in color, go online.

Diffusion state classification

We noticed that the gyration method has higher correctness and is more robust compared to the other tested methods, especially in situations with higher localization errors ($\sigma_{xy} = 40$ nm). The reason may be found in the fact that more information is used to determine the gyration radius compared to the value calculated with the windowed MSD or the MLE methods. In the calculation of the gyration, the information of the distances between all the segments positions is taken into account unlike in MLE. Therefore, the gyration method not only considers the distance between points, but also the relative locations of the positions. For example, for pure diffusion, it is unlikely that a particle would move in only one direction. The MLE would not detect this, because it only considers subsequent distances; however, the gyration method will detect it. The spatial information of relative location of the positions is only considered in the gyration and confinement methods, which might be the reason why these methods scored higher in classification of the two diffusion states. In the windowed MSD method, the optimum result is obtained when the fit to find the diffusion value is obtained from information only up to a time lag of three frames. This means that in the case of the windowed MSD calculation, the distance information from the first to the last point is not considered, whereas this is taken into account in the gyration method. However, when the positions are more precisely known (i.e., low localization error), the MLE and Bayesian-based methods start to outperform the gyration method. An explanation for this might lie in the fact that these methods make use of averaged distances of single steps. The average value of single steps in a segment is apparently precise enough to find the most likely underlying diffusion coefficient. Without localization errors, the (windowed) MSD also scores best when only single steps (corresponding to a time lag of one frame) are considered. Our approach with

the windowed MSD is then in fact equivalent to the MLE method (43). Another reason why the windowed MSD scores lower than other methods might be because MSD values can be negative, especially with higher localization errors. It is not clear what the chance is that negative values represent a slow or a fast state (we classified these values as slow), such that negative values cannot be adequately classified.

Interestingly, it remains an open question whether the gyration-based classification method is the optimal quantification measure for the cases simulated, or if another quantification measure can be invented that outperforms gyration-based classification. We saw that classification based on the maximum likelihood of the average of single step sizes is outperformed by gyration-based classification, hence MLE does not yield the optimal performance to this problem. How to best combine all the positional information of a segment remains an open question.

Although we demonstrated the state classification for a two-population system, the framework and the methods can also be used for more than two populations. The CDF fit should then be adjusted for multiple populations, and thresholds can similarly be set at the found αth percentile. This expansion can be benchmarked using simulation situations comparable to those we have presented here. Other quantification methods can also use this framework for benchmarking the method in a realistic context of single molecule experiment on plasma membrane receptors. In this article we have tested prevalent analysis methods for quantification of the local diffusion. Although the confinement and gyration methods have been developed in the context of confinement, they had never been applied for quantification of pure Brownian motion, whereas we showed that these methods outperform classical methods to classify segments to a diffusion state.

Michalet (34) has discussed the practicality of using a windowed MSD. He argued that the segment length must be chosen small enough so as to measure local behavior and not averaged global behavior, yet must still be large enough to be sufficiently accurate inasmuch as too-small windows have a broad distribution in output values. He therefore concluded that this method can rarely provide reliable estimates of the diffusion coefficients, and can only show a difference in multiple orders of magnitude, even for windows of 100 points. Although this conclusion is valid in the case of exceedingly low diffusion coefficients, such as $D = 10^{-4}$ μm^2/s in his example, we showed that a windowed MSD can still be useful in diffusion-state classification. However, it is indeed not as powerful as the other methods tested.

We chose to use the CDF-fit approach to find the global diffusion values. Another approach to obtain the diffusion coefficients has been described using Bayesian statistics (45) and a hidden Markov model. This method finds the different (and hidden number of) diffusion states with their diffusion coefficients (40). Although this method yields accurate results, it also requires about a thousandfold more computational time on our computer, whereas a CDF fit is comparably accurate. Concerning the accuracy of the quantification measure, we neglected the influence of the exposure time on these values. Whereas this leads to underestimation of the value of the diffusion coefficient due to the averaging blur during exposure (1,48), we only used the values to classify states; the exposure time effect should not have much influence on this classification.

We only regarded spatiotemporal analysis methods in this article, because the spatial information may yield especially important information, such as where a molecule is interacting. Therefore, we have excluded image correlation spectroscopy methods (such as particle image correlation spectroscopy (49,50)) that do not require tracking, and a Monte Carlo approach (38). Also, we only looked at alternating diffusion states, and not at active transport or confinement, as explained before.

Application in live cells

The application of the gyration-based diffusion-state classification approach demonstrated that the correctness achieved is sufficient to identify spatial zones of slowed diffusion within cellular structures. Such zones are particularly important because they reflect the regions where the protein interacts with other proteins or cellular compounds. The physiological meaning of the slow diffusion zones in our example of EGF receptor remains an open question at the moment. They could be related to cytoskeletal structures or regions where the receptor exhibits internalization. For other proteins, we might find another distribution of membrane patches of slowed diffusion, and specific diffusion states near other cellular structures such as actin or microtubuli might be seen. In that case, single molecule trajectories may indicate a role of such cellular structures in the signaling of the protein studied when analyzed by diffusion-state classification.

Diffusion-state lifetimes obtained by this classification framework seem less informative, as they tend to be underestimated due to short periods of incorrect state classification (see Fig. S5). To reliably obtain changes in state lifetimes, a high classification correctness (>85%) seems essential. However, state lifetimes can be used as a test to confirm that the diffusive populations found (using the CDF fit) are lasting longer than the timescale of the sampling rate (time between frames). States with extremely short lifetimes are probably caused by issues with multiple intermixed diffusive states, and further diffusion classification is unreliable in that case.

CONCLUSION

In summary, we have introduced what we believe is a new strategy for spatiotemporal classification of two-population

diffusion, and compared methods to be used for this classification. We have validated our proposed diffusion-state classification approach by testing with simulations and showed possible applications, such as determining diffusion-state lifetimes and composing diffusion-state images. The key feature of the proposed framework is that a diffusion estimator is the logical choice but not necessarily the best way to discriminate and classify segments to two diffusion states. When we have determined the diffusion coefficients and their fractions present in the motion of all the molecules (e.g., using a CDF fit of the squared displacements (20)), there is no need to find a local diffusion coefficient. What remains is the need to classify the local motion to one of the found diffusion states. The found fraction size α can be used to perform objective thresholding of the local quantification measures. This avoids relying on subjective manual thresholding in segment-based methods to detect transitions between motion patterns (39), such as relative confinement (4,36).

We have found that the gyration method is best used for diffusion-state classification when the localization error (due to photon shot noise and the finite proximity of the fluorescent dye to the protein) is ~40 nm, whereas MLE or Bayesian methods are preferred in the case of localization errors of 20 nm or less. Although the differences in the resulting classification correctness are small, the robustness of the gyration method is higher than the MLE method, especially when a limited number of displacements are available for the CDF fit. Furthermore, the Bayesian method was approximately a thousandfold slower on our computer, whereas it outperforms the gyration-based classification only marginally. For realistic plasma membrane receptor motion, the optimal setting of the gyration method requires a segment window of 4–7 frames; the method then classifies 70–90% correct, depending on the exact characteristics of the motion. Simulations with spatially organized diffusion states demonstrated that this is adequate to observe spatial organization of diffusion states. The estimated correctness for experimental data may be determined by performing simulations as demonstrated. When the diffusion states are visualized at high resolution at their position in live cells, such diffusion-state images may aid in identifying spatially separated zones of the occurring states on the membrane of the cell. Zones of slowed diffusion are an indication of interactions with the protein studied. We showed that such zones exist for EGF receptors within cellular structures. The image also showed static or slowly dynamic cellular structures, such as filopodia.

In conclusion, new biophysical insights could be acquired from spatiotemporal information of protein mobility. Such information can be obtained through the proposed diffusion-state classification approach. We expect that the visualization of zones of altered diffusion of proteins on top of other cellular structures will help in providing a better understanding in the organization of the plasma membrane and the role of the cytoskeleton in protein signaling. Spatial diffusion classification will be a valuable tool for obtaining more insight into the complex protein interactions in live cells.

SUPPORTING MATERIAL

Thirteen figures, one table, analysis software, and three movies are available at http://www.biophysj.org/biophysj/supplemental/S0006-3495(14)00682-1.

The authors thank Kasper van Zon for discussions about the state classification likelihood, and Jenny Ibach from the Verveer group at the Max Planck Institute of Molecular Physiology for providing the SNAP-ErbB1 plasmid. We also thank Peter Relich and Dr. Keith Lidke from the University of New Mexico for sharing their single molecule tracking software with us.

This work is supported by the ERA-NET NanoSci E+ program via Stichting Technische Wetenschappen grant No. 11022-NanoActuate.

SUPPORTING CITATIONS

References (51–55) appear in the Supporting Material.

REFERENCES

1. Goulian, M., and S. M. Simon. 2000. Tracking single proteins within cells. *Biophys. J.* 79:2188–2198.
2. Sako, Y., S. Minoghchi, and T. Yanagida. 2000. Single molecule imaging of EGFR signaling on the surface of living cells. *Nat. Cell Biol.* 2:168–172.
3. Wieser, S., and G. J. Schütz. 2008. Tracking single molecules in the live cell plasma membrane—do's and don't's. *Methods.* 46:131–140.
4. Sergé, A., N. Bertaux, …, D. Marguet. 2008. Dynamic multiple-target tracing to probe spatiotemporal cartography of cell membranes. *Nat. Methods.* 5:687–694.
5. Holtzer, L., and T. Schmidt. 2010. The tracking of individual molecules in cells and tissues. *In* Single Particle Tracking and Single Molecule Energy Transfer. C. Bräuchle, D. C. Lamb, and J. Michaelis, editors. Wiley-VCH Verlag, Weinheim, Germany.
6. Low-Nam, S. T., K. A. Lidke, …, D. S. Lidke. 2011. ErbB1 dimerization is promoted by domain co-confinement and stabilized by ligand binding. *Nat. Struct. Mol. Biol.* 18:1244–1249.
7. Lippincott-Schwartz, J., E. Snapp, and A. Kenworthy. 2001. Studying protein dynamics in living cells. *Nat. Rev. Mol. Cell Biol.* 2:444–456.
8. Miyawaki, A. 2011. Proteins on the move: insights gained from fluorescent protein technologies. *Nat. Rev. Mol. Cell Biol.* 12:656–668.
9. Giepmans, B. N. G., S. R. Adams, …, R. Y. Tsien. 2006. The fluorescent toolbox for assessing protein location and function. *Science.* 312:217–224.
10. Kusumi, A., C. Nakada, …, T. Fujiwara. 2005. Paradigm shift of the plasma membrane concept from the two-dimensional continuum fluid to the partitioned fluid: high-speed single molecule tracking of membrane molecules. *Annu. Rev. Biophys. Biomol. Struct.* 34:351–378.
11. Cambi, A., and D. S. Lidke. 2012. Nanoscale membrane organization: where biochemistry meets advanced microscopy. *ACS Chem. Biol.* 7:139–149.
12. Sako, Y., and T. Yanagida. 2003. Single molecule visualization in cell biology. *Nat. Rev. Mol. Cell Biol.* 4 (*Suppl*):SS1–SS5.
13. Saxton, M. J., and K. Jacobson. 1997. Single particle tracking: applications to membrane dynamics. *Annu. Rev. Biophys. Biomol. Struct.* 26:373–399.
14. Engelman, D. M. 2005. Membranes are more mosaic than fluid. *Nature.* 438:578–580.

15. Shaw, A. S. 2006. Lipid rafts: now you see them, now you don't. *Nat. Immunol.* 7:1139–1142.

16. Jacobson, K., O. G. Mouritsen, and R. G. W. Anderson. 2007. Lipid rafts: at a crossroad between cell biology and physics. *Nat. Cell Biol.* 9:7–14.

17. Citri, A., and Y. Yarden. 2006. EGF-ERBB signaling: towards the systems level. *Nat. Rev. Mol. Cell Biol.* 7:505–516.

18. Lemmon, M. A., and J. Schlessinger. 2010. Cell signaling by receptor tyrosine kinases. *Cell.* 141:1117–1134.

19. Kapanidis, A. N., and T. Strick. 2009. Biology, one molecule at a time. *Trends Biochem. Sci.* 34:234–243.

20. Schütz, G. J., H. Schindler, and T. Schmidt. 1997. Single molecule microscopy on model membranes reveals anomalous diffusion. *Biophys. J.* 73:1073–1080.

21. Brameshuber, M., and G. J. Schütz. 2012. In Vivo Tracking of Single Biomolecules: What Trajectories Tell Us About the Acting Forces. Springer Series on Fluorescence, Springer, Berlin, Germany, pp. 1–37.

22. Dietrich, C., B. Yang, …, K. Jacobson. 2002. Relationship of lipid rafts to transient confinement zones detected by single particle tracking. *Biophys. J.* 82:274–284.

23. de Keijzer, S., A. Sergé, …, B. E. Snaar-Jagalska. 2008. A spatially restricted increase in receptor mobility is involved in directional sensing during *Dictyostelium discoideum* chemotaxis. *J. Cell Sci.* 121:1750–1757.

24. Cebecauer, M., M. Spitaler, …, A. I. Magee. 2010. Signaling complexes and clusters: functional advantages and methodological hurdles. *J. Cell Sci.* 123:309–320.

25. Harding, A. S., and J. F. Hancock. 2008. Using plasma membrane nanoclusters to build better signaling circuits. *Trends Cell Biol.* 18:364–371.

26. Harding, A., and J. F. Hancock. 2008. Ras nanoclusters: combining digital and analog signaling. *Cell Cycle.* 7:127–134.

27. Kholodenko, B. N., J. F. Hancock, and W. Kolch. 2010. Signaling ballet in space and time. *Nat. Rev. Mol. Cell Biol.* 11:414–426.

28. Radhakrishnan, K., Á. Halász, …, B. S. Wilson. 2012. Mathematical simulation of membrane protein clustering for efficient signal transduction. *Ann. Biomed. Eng.* 40:2307–2318.

29. Xiao, Z., W. Zhang, …, X. Fang. 2008. Single molecule diffusion study of activated EGFR implicates its endocytic pathway. *Biochem. Biophys. Res. Commun.* 369:730–734.

30. Rong, G., and B. M. Reinhard. 2012. Monitoring the size and lateral dynamics of ErbB1 enriched membrane domains through live cell plasmon coupling microscopy. *PLoS ONE.* 7:e34175.

31. Orr, G., D. Hu, …, S. D. Colson. 2005. Cholesterol dictates the freedom of EGF receptors and HER2 in the plane of the membrane. *Biophys. J.* 89:1362–1373.

32. Manley, S., J. M. Gillette, …, J. Lippincott-Schwartz. 2008. High-density mapping of single molecule trajectories with photoactivated localization microscopy. *Nat. Methods.* 5:155–157.

33. Kusumi, A., Y. Sako, and M. Yamamoto. 1993. Confined lateral diffusion of membrane receptors as studied by single particle tracking (nanovid microscopy). Effects of calcium-induced differentiation in cultured epithelial cells. *Biophys. J.* 65:2021–2040.

34. Michalet, X. 2010. Mean square displacement analysis of single particle trajectories with localization error: Brownian motion in an isotropic medium. *Phys. Rev. E Stat. Nonlin. Soft Matter Phys.* 82:041914.

35. Simson, R., E. D. Sheets, and K. Jacobson. 1995. Detection of temporary lateral confinement of membrane proteins using single particle tracking analysis. *Biophys. J.* 69:989–993.

36. Meilhac, N., L. Le Guyader, …, N. Destainville. 2006. Detection of confinement and jumps in single molecule membrane trajectories. *Phys. Rev. E Stat. Nonlin. Soft Matter Phys.* 73:011915.

37. Elliott, L. C. C., M. Barhoum, …, P. W. Bohn. 2011. Trajectory analysis of single molecules exhibiting non-Brownian motion. *Phys. Chem. Chem. Phys.* 13:4326–4334.

38. Wieser, S., M. Axmann, and G. J. Schütz. 2008. Versatile analysis of single molecule tracking data by comprehensive testing against Monte Carlo simulations. *Biophys. J.* 95:5988–6001.

39. Helmuth, J. A., C. J. Burckhardt, …, I. F. Sbalzarini. 2007. A novel supervised trajectory segmentation algorithm identifies distinct types of human adenovirus motion in host cells. *J. Struct. Biol.* 159:347–358.

40. Persson, F., M. Lindén, …, J. Elf. 2013. Extracting intracellular diffusive states and transition rates from single molecule tracking data. *Nat. Methods.* 10:265–269.

41. Jaqaman, K., H. Kuwata, …, S. Grinstein. 2011. Cytoskeletal control of CD36 diffusion promotes its receptor and signaling function. *Cell.* 146:593–606.

42. Bouzigues, C., and M. Dahan. 2007. Transient directed motions of $GABA_A$ receptors in growth cones detected by a speed correlation index. *Biophys. J.* 92:654–660.

43. Montiel, D., H. Cang, and H. Yang. 2006. Quantitative characterization of changes in dynamical behavior for single-particle tracking studies. *J. Phys. Chem. B.* 110:19763–19770.

44. Ott, M., Y. Shai, and G. Haran. 2013. Single-particle tracking reveals switching of the HIV fusion peptide between two diffusive modes in membranes. *J. Phys. Chem. B.* 117:13308–13321.

45. Eddy, S. R. 2004. What is Bayesian statistics? *Nat. Biotechnol.* 22:1177–1178.

46. Lidke, D. S., P. Nagy, …, T. M. Jovin. 2004. Quantum dot ligands provide new insights into erbB/HER receptor-mediated signal transduction. *Nat. Biotechnol.* 22:198–203.

47. Arndt-Jovin, D. 2006. Quantum dots shed light on processes in living cells. 9 July 2006, SPIE Newsroom. http://dx.doi.org/10.1117/2.1200605.0228.

48. Berglund, A. J. 2010. Statistics of camera-based single-particle tracking. *Phys. Rev. E Stat. Nonlin. Soft Matter Phys.* 82:011917.

49. Semrau, S., and T. Schmidt. 2007. Particle image correlation spectroscopy (PICS): retrieving nanometer-scale correlations from high-density single-molecule position data. *Biophys. J.* 92:613–621.

50. Semrau, S., L. Holtzer, …, T. Schmidt. 2011. Quantification of biological interactions with particle image cross-correlation spectroscopy (PICCS). *Biophys. J.* 100:1810–1818.

51. Qian, H., M. P. Sheetz, and E. L. Elson. 1991. Single particle tracking. Analysis of diffusion and flow in two-dimensional systems. *Biophys. J.* 60:910–921.

52. Saxton, M. J. 1993. Lateral diffusion in an archipelago. Single-particle diffusion. *Biophys. J.* 64:1766–1780.

53. Saxton, M. J. 1997. Single particle tracking: the distribution of diffusion coefficients. *Biophys. J.* 72:1744–1753.

54. Smith, C. S., N. Joseph, …, K. A. Lidke. 2010. Fast, single molecule localization that achieves theoretically minimum uncertainty. *Nat. Methods.* 7:373–375.

55. Brauchle, C., D.C. Lamb, and J. Michaelis. Single Particle Tracking and Single Molecule Energy Transfer. Wiley-VCH Verlag, Weinheim, Germany.

Supporting Material for

Classification of dynamical diffusion states in single molecule tracking microscopy

P.J. Bosch[†], J.S. Kanger[‡] and V. Subramaniam[†‡#]

[†] Nanobiophysics, MESA+ Institute for Nanotechnology, University of Twente, The Netherlands
[‡] MIRA Institute for Biomedical Technology and Technical Medicine, University of Twente, The Netherlands
[#] Present address: FOM Institute AMOLF, Science Park 104, 1098 XG Amsterdam, The Netherlands

Contents

Supporting Figures

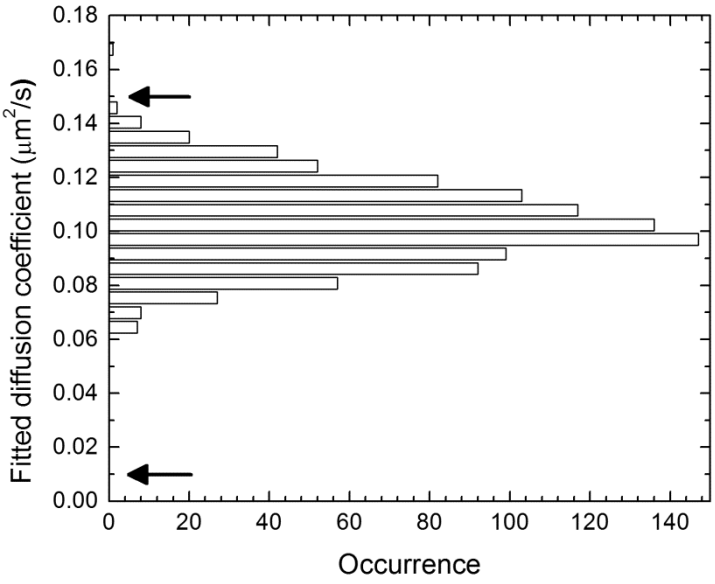

FIGURE S1: A conventional full-trajectory MSD analysis of a two-population diffusion systems leads to an apparent distribution of diffusion values, easily resulting in erroneous conclusions for this motion system. The true motion system is a two-population diffusion system with diffusion coefficients of 0.15 and 0.01 $\mu m^2/s$, as indicated by the arrows in the graph. For this graph, 1000 trajectories consisting of 500 frames (hence relatively long trajectories) were simulated. The trajectories are analyzed using the conventional full-trajectory MSD method, where the first 4 points of the MSD curve were used following the "rule of thumb" rule to fit the diffusion constant. The found diffusion constants and the apparent spread both incorrectly describe this two-population situation. The MSD analysis should therefore only be used for homogeneous (one-population) motion. The discussion further in the supplementary material discusses the accuracy of determining the diffusion constant for a one-population system using the full-trajectory MSD method.

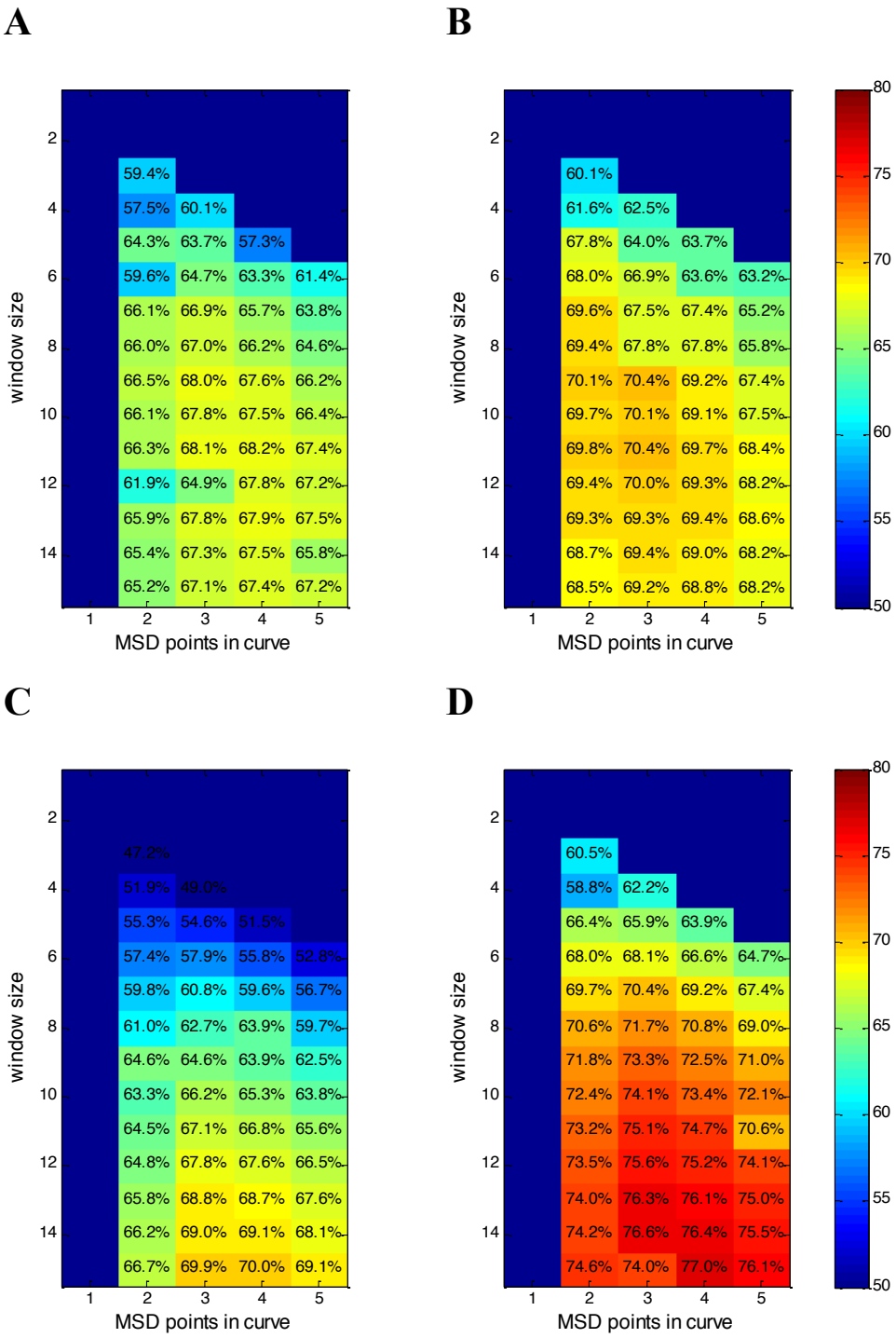

FIGURE S2: Correctness dependence of window length and of the number of points in the MSD curve used to fit the diffusion value. (*A*) Simulation case A has a localization inaccuracy σ_{xy} of 40nm and short state lifetimes (τ_1 = τ_2 = 300 ms). (*B*) This simulation case differs from case A only by a lowered localization inaccuracy σ_{xy} = 20nm. (*C*) This simulation case differs from case A only by having longer fast state lifetimes (τ_1 = 900 ms; τ_2 = 300 ms; σ_{xy} = 40nm). (*D*) This simulation case also has longer slow state lifetimes (τ_1 = 900 ms; τ_2 = 900 ms; σ_{xy} = 40nm). The color bar aids in reading the classification correctness percentage.

A

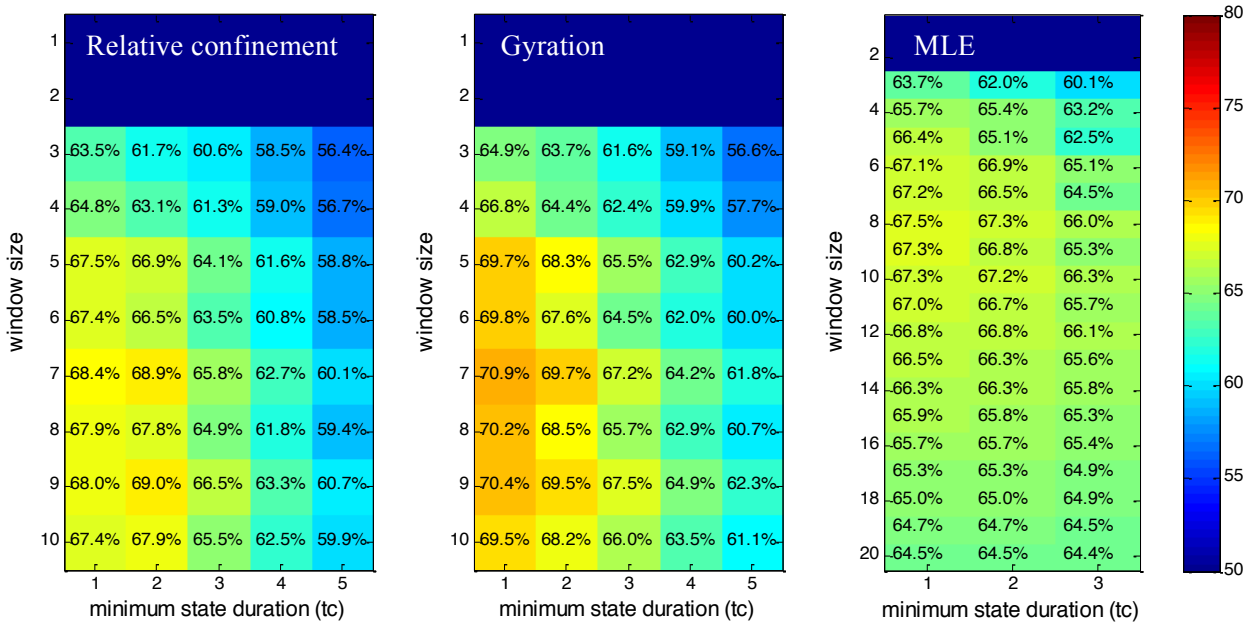
Relative confinement
window size
minimum state duration (tc)
1 2 3 4 5
3 63.5% 61.7% 60.6% 58.5% 56.4%
4 64.8% 63.1% 61.3% 59.0% 56.7%
5 67.5% 66.9% 64.1% 61.6% 58.8%
6 67.4% 66.5% 63.5% 60.8% 58.5%
7 68.4% 68.9% 65.8% 62.7% 60.1%
8 67.9% 67.8% 64.9% 61.8% 59.4%
9 68.0% 69.0% 66.5% 63.3% 60.7%
10 67.4% 67.9% 65.5% 62.5% 59.9%
Gyration
window size
minimum state duration (tc)
1 2 3 4 5
3 64.9% 63.7% 61.6% 59.1% 56.6%
4 66.8% 64.4% 62.4% 59.9% 57.7%
5 69.7% 68.3% 65.5% 62.9% 60.2%
6 69.8% 67.6% 64.5% 62.0% 60.0%
7 70.9% 69.7% 67.2% 64.2% 61.8%
8 70.2% 68.5% 65.7% 62.9% 60.7%
9 70.4% 69.5% 67.5% 64.9% 62.3%
10 69.5% 68.2% 66.0% 63.5% 61.1%
MLE
window size
minimum state duration (tc)
1 2 3
2 63.7% 62.0% 60.1%
4 65.7% 65.4% 63.2%
6 66.4% 65.1% 62.5%
8 67.1% 66.9% 65.1%
10 67.2% 66.5% 64.5%
12 67.5% 67.3% 66.0%
14 67.3% 66.8% 65.3%
16 67.3% 67.2% 66.3%
18 67.0% 66.7% 65.7%
20 66.8% 66.8% 66.1%
66.5% 66.3% 65.6%
66.3% 66.3% 65.8%
65.9% 65.8% 65.3%
65.7% 65.7% 65.4%
65.3% 65.3% 64.9%
65.0% 65.0% 64.9%
64.7% 64.7% 64.5%
64.5% 64.5% 64.4%
80 75 70 65 60 55 50

B

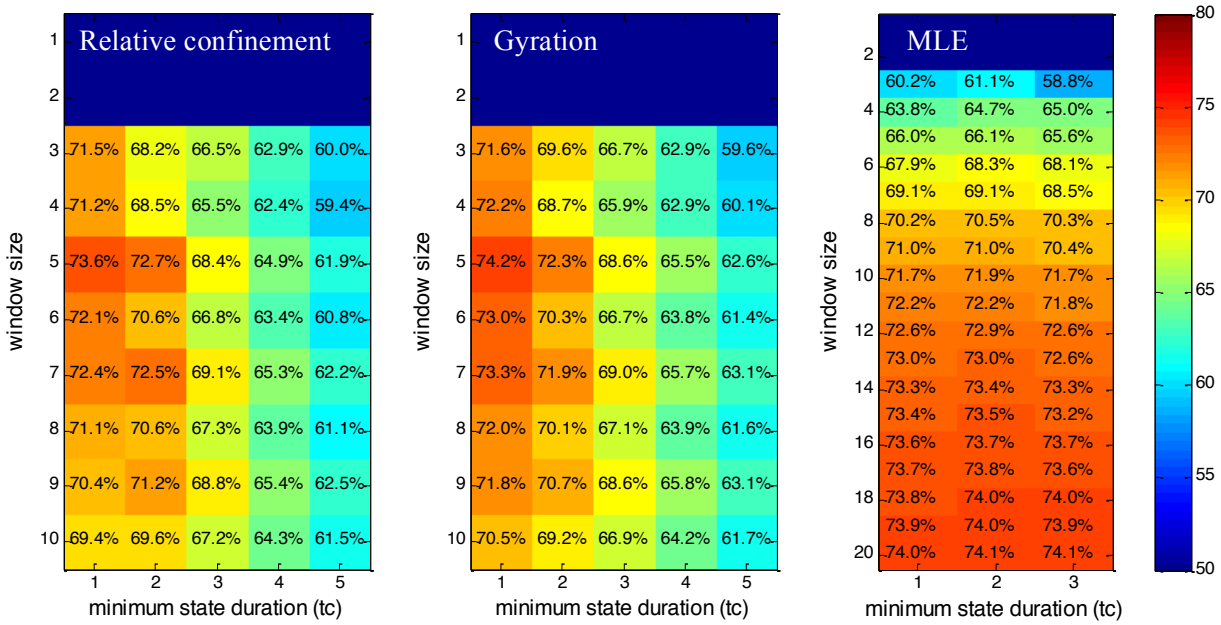
Relative confinement
window size
minimum state duration (tc)
1 2 3 4 5
3 71.5% 68.2% 66.5% 62.9% 60.0%
4 71.2% 68.5% 65.5% 62.4% 59.4%
5 73.6% 72.7% 68.4% 64.9% 61.9%
6 72.1% 70.6% 66.8% 63.4% 60.8%
7 72.4% 72.5% 69.1% 65.3% 62.2%
8 71.1% 70.6% 67.3% 63.9% 61.1%
9 70.4% 71.2% 68.8% 65.4% 62.5%
10 69.4% 69.6% 67.2% 64.3% 61.5%
Gyration
window size
minimum state duration (tc)
1 2 3 4 5
3 71.6% 69.6% 66.7% 62.9% 59.6%
4 72.2% 68.7% 65.9% 62.9% 60.1%
5 74.2% 72.3% 68.6% 65.5% 62.6%
6 73.0% 70.3% 66.7% 63.8% 61.4%
7 73.3% 71.9% 69.0% 65.7% 63.1%
8 72.0% 70.1% 67.1% 63.9% 61.6%
9 71.8% 70.7% 68.6% 65.8% 63.1%
10 70.5% 69.2% 66.9% 64.2% 61.7%
MLE
window size
minimum state duration (tc)
1 2 3
2 60.2% 61.1% 58.8%
4 63.8% 64.7% 65.0%
6 66.0% 66.1% 65.6%
8 67.9% 68.3% 68.1%
10 69.1% 69.1% 68.5%
12 70.2% 70.5% 70.3%
14 71.0% 71.0% 70.4%
16 71.7% 71.9% 71.7%
18 72.2% 72.2% 71.8%
20 72.6% 72.9% 72.6%
73.0% 73.0% 72.6%
73.3% 73.4% 73.3%
73.4% 73.5% 73.2%
73.6% 73.7% 73.7%
73.7% 73.8% 73.6%
73.8% 74.0% 74.0%
73.9% 74.0% 73.9%
74.0% 74.1% 74.1%
80 75 70 65 60 55 50

C

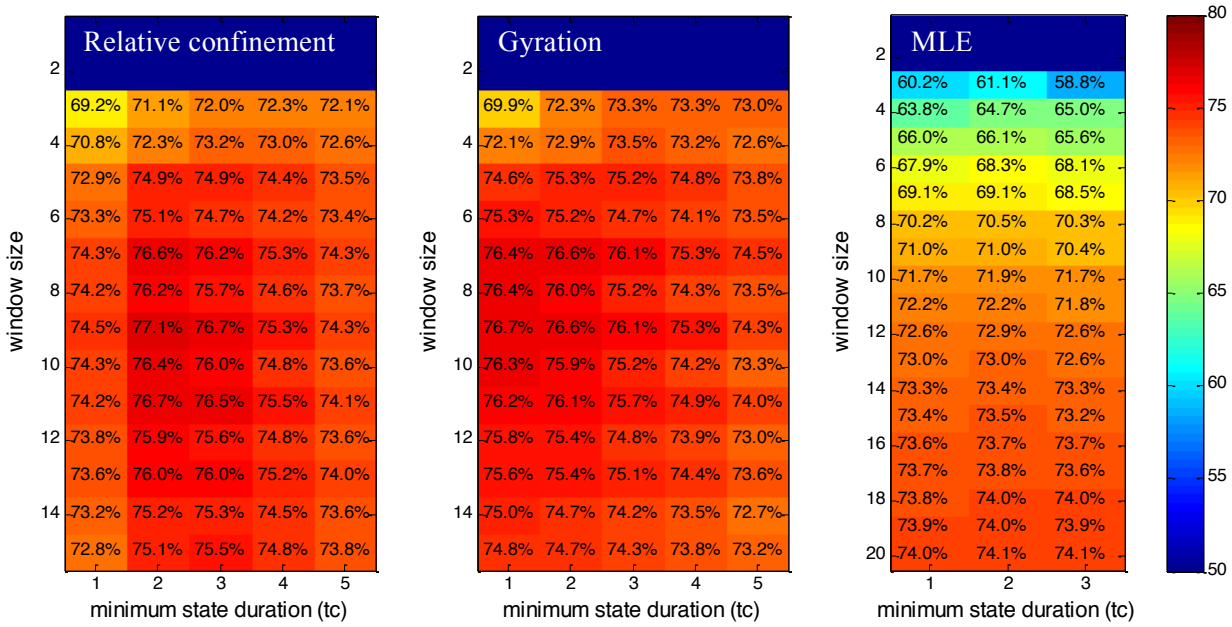

D

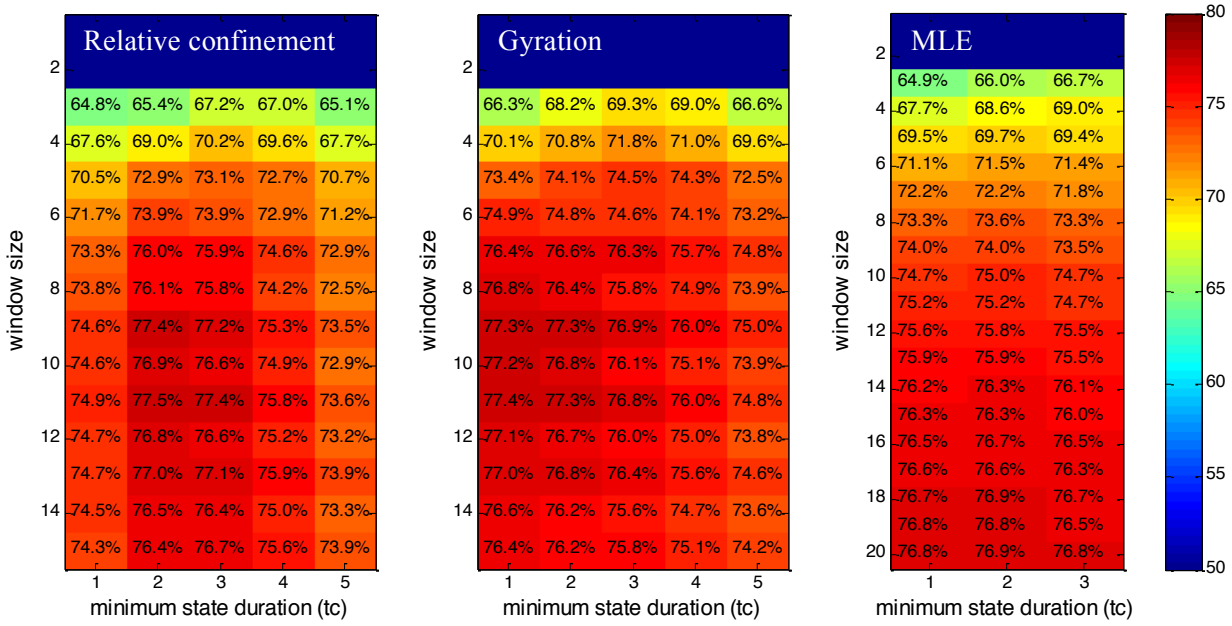

FIGURE S3: Effect of a minimum state duration filter on classification correctness. Since all the above methods make use of segments, the state classification does not allocate exact time points of a trajectory to a state, but to a window of several time points. The state of this window is classified at the center time point of the window, and thereby each time point has its own state allocation based on different but correlated data sets. Now the state classification is defined at all timepoints except for the beginning and end of a (sub)trajectory. Since the window is several frames long, state durations shorter than the segment length (window size) may appear illogical, and therefore we also tested whether filtering out short state durations leads to better correctness for different classification methods. In most simulation cases (as described in the main text) this was not the case, and we have therefore looked only at unfiltered state classifications in the main text. (*A-D*) Classification correctness for simulation case A-D. The color bar aids in reading the classification correctness percentage.

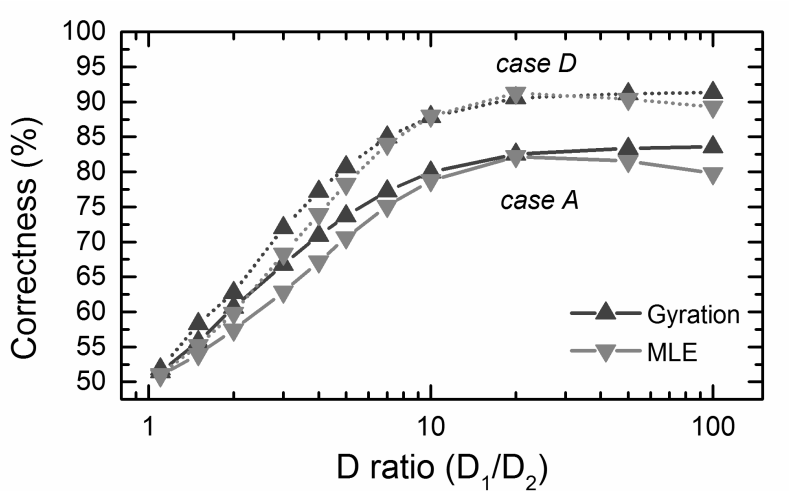

FIGURE S4: Correctness of the two-population classification for different ratios for D_1 and D_2. D_2 was kept fixed at 0.015 $\mu m^2/s$. Shown are the results for a gyration and MLE based classification for simulations of cases A and D (with changing D_1). We find that ratio of 4 in our simulation cases was indeed a challenging situation, and that with ratios larger than 10 the best achievable classification are obtained. The classification also depends on other factors as shown by the different results for the two cases shown.

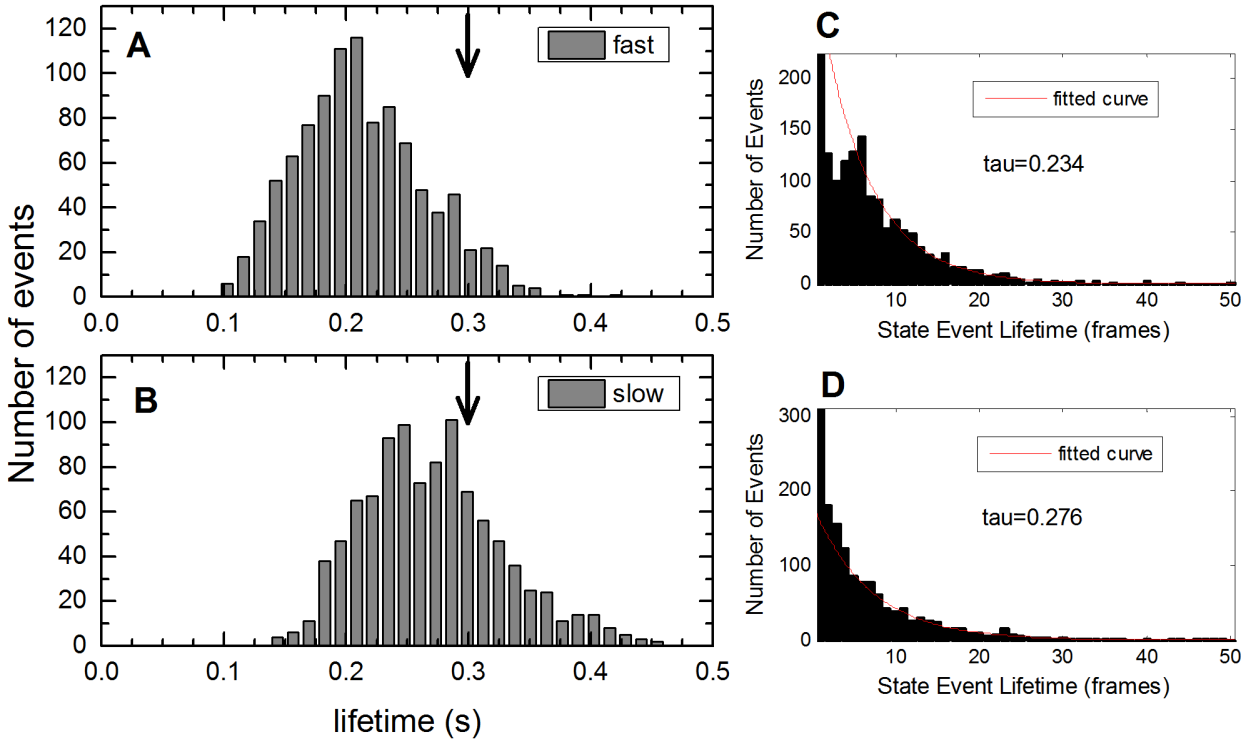

FIGURE S5: The distribution of lifetimes found by the gyration based classification method simulation case A. The simulation consisted of 20 trajectories and was repeated 1,000 times to yield the distribution of lifetimes of the slow state (*A*) and the fast state (*B*). The gyration method used a segment length of 7 frames. The arrows indicate the true lifetime of both states. (*C*) Example of a lifetime fit of the fast state from one simulation. This fit is only performed over state events larger than 5 frames. (*D*) Example of a fit of the slow state. This fit is only performed over state events larger than 5 frames. Although the lifetimes found are not too far off in this case, in cases with longer state durations (such as case D), the lifetimes found are significantly underestimated.

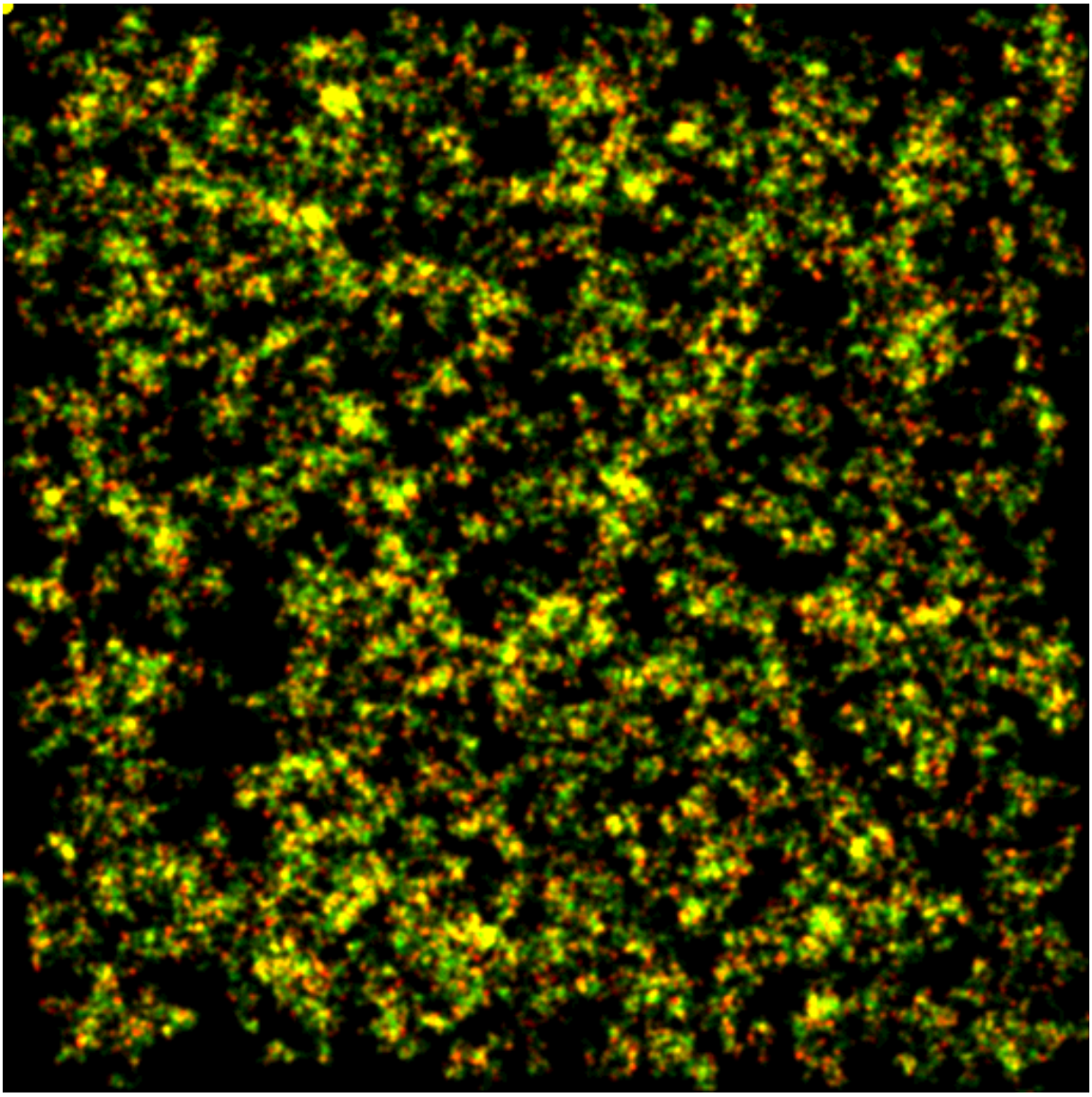

FIGURE S6: Image reconstruction of the state classification distribution of simulation case A. In this case there were as many slow as fast states. The dimension of the image is 55x55µm, and the image is reconstructed at 60nm/pixel.

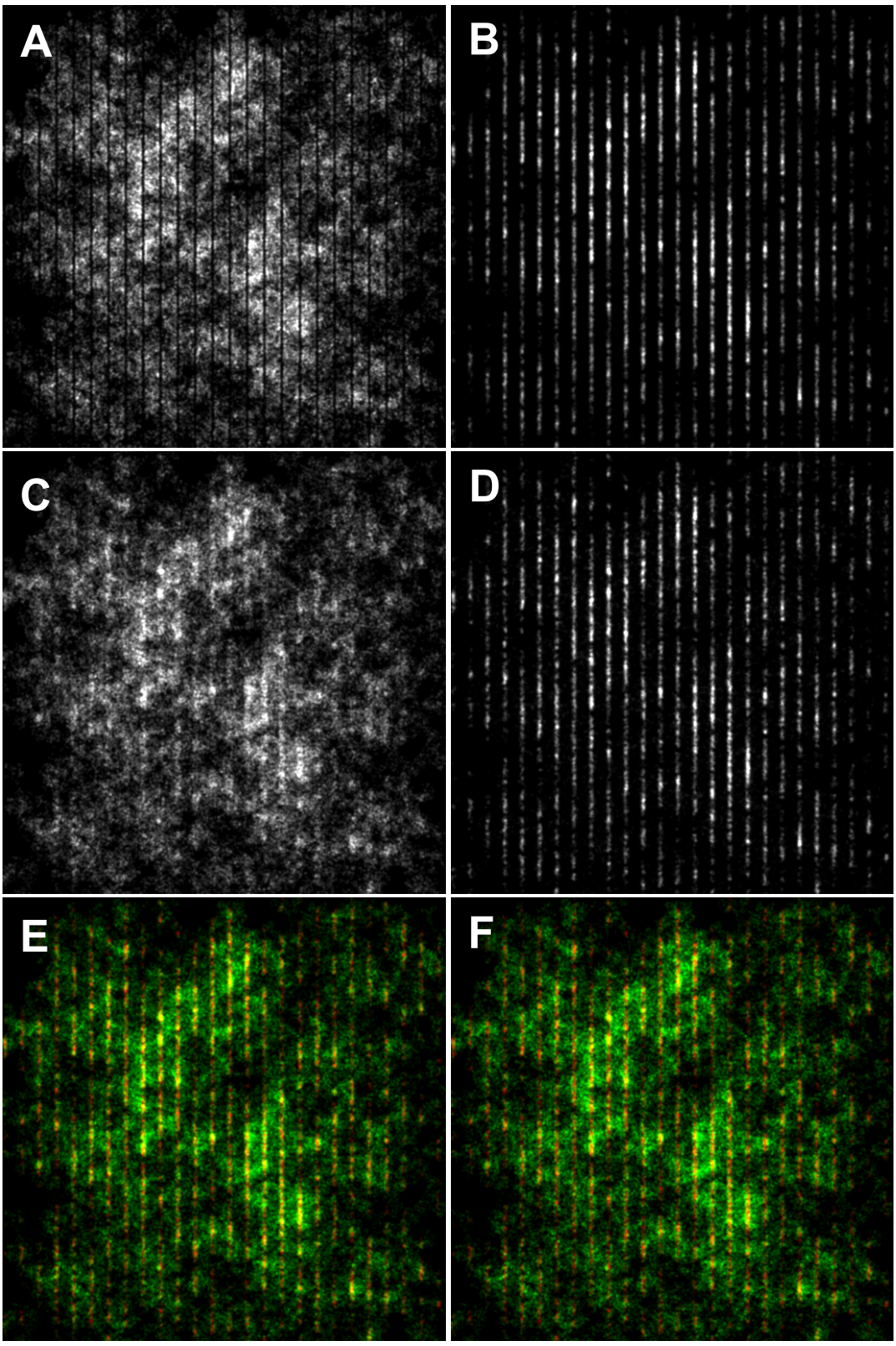

FIGURE S7: Image reconstructions of the state classification distribution of a simulation with spatially defined diffusion states. (*A*) Simulation (actual) image of fast state. (*B*) Simulation (actual) image of slow state. (*C*) Fast state image found by MLE method. (*D*) Slow state image found by MLE method. (*E*) Colour image of states map as found by the MLE method. Green represents fast state, and red represents slow state. (*F*) Colour image of states map as found by the gyration method. Green represents fast state, and red represents slow state. A segment length of 4 frames was used in both classification methods (this value yielded the highest correctness). The dimension of the image is 15x15µm, and the image is reconstructed at 30nm/pixel.

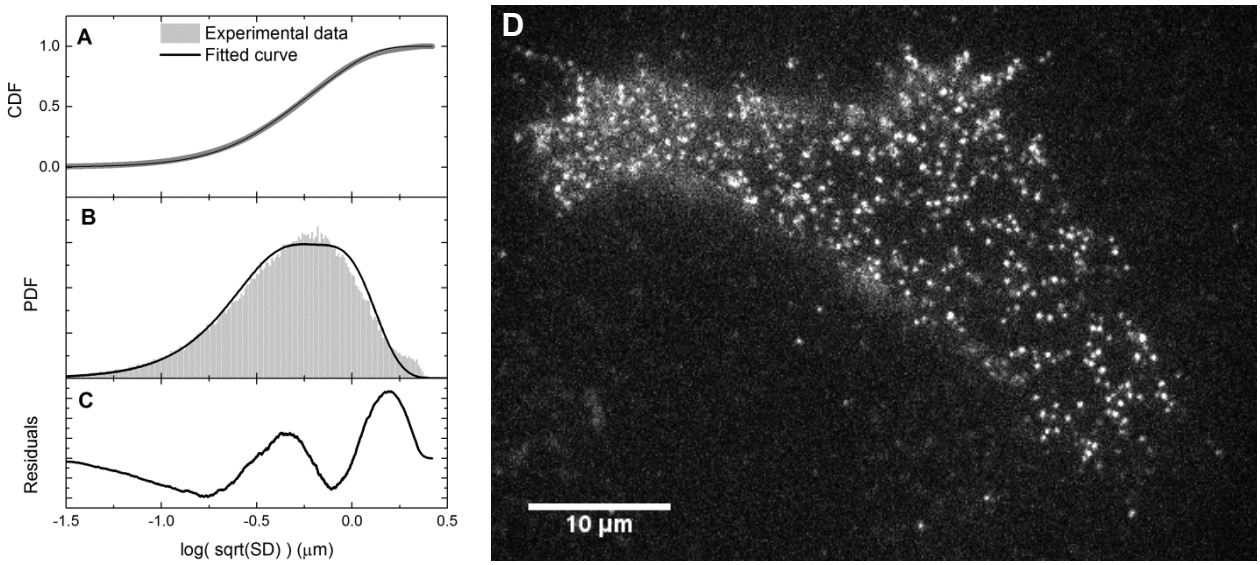

FIGURE S8: The proposed approach for diffusion state classification applied to experimental data. (*A*) The CDF fit, with corresponding PDF (*B*) and residuals (*C*), for the motion of EGF receptor in an MCF7 cell shows that the model of two-population Brownian diffusion is a suitable motion model. (D) An example of a single molecule fluorescence frame recording of EGF receptor in an MCF7 cell. The image has not been modified or filtered.

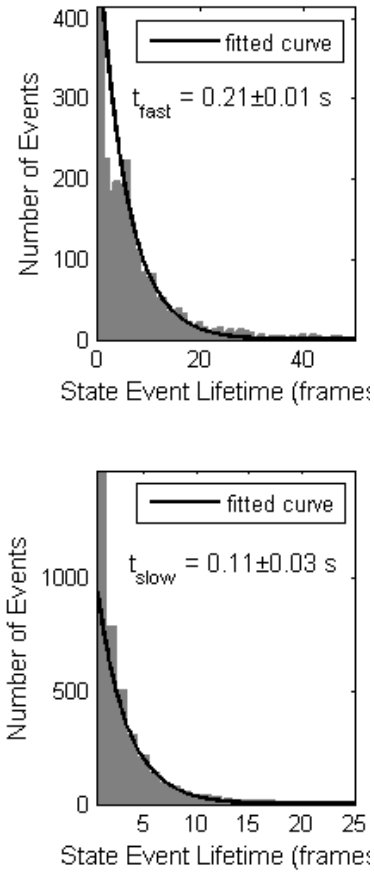

FIGURE S9: Histograms of unliganded EGF receptor state lifetimes for the fast state (*upper*) and the slow state (*lower*) in frames (video was recorded at 25 fps), determined by gyration analysis. The characteristic lifetime is determined from an exponential fit of state durations longer than 5 frames, since the use of a segment length of 7 frames does not correctly resolve shorter lifetimes. The state duration will be underestimated because of random incorrect state classification.

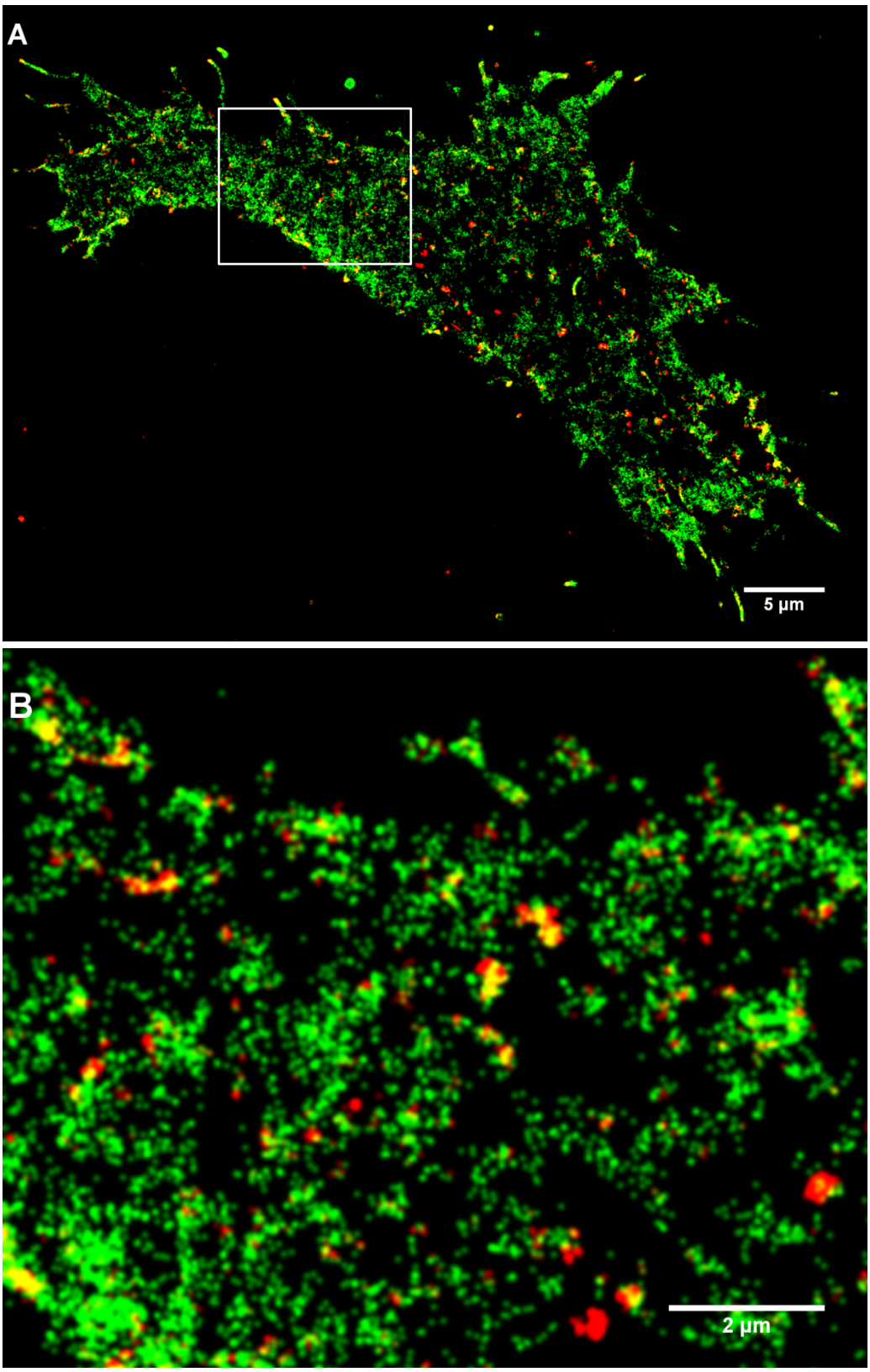

FIGURE S10: Image reconstructions of the distribution of states exhibited by liganded EGF receptor proteins in an MCF7 cell. The resolution of the reconstructed images is 30nm/pixel. (*A*) Image showing the areas travelled by receptors in the fast diffusion state (green), and areas where receptors in the slow diffusion state were detected (red). (*B*) Zoomed image of the indicated area (white box) in *A*.

Supporting Sections

Quantification measures

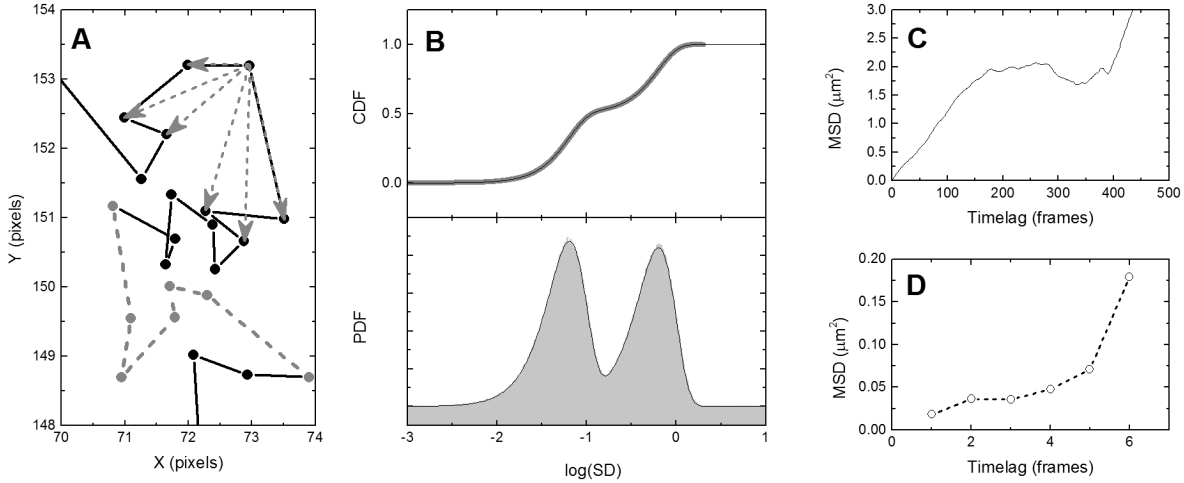

FIGURE S11: Illustrations of various segment analysis methods as quantification measures for the proposed diffusion state classification approach. (*A*) Simulated two-population diffusion trajectory and examples of selected information for the relative confinement and the gyration method on a trajectory segment. Relative confinement detection takes the variance of distances from the center of the segment (indicated by the grey arrows). The gyration radius depends on the variance and covariance of the coordinates (segment indicated in grey with a dashed line). (*B*) Cumulative distribution function (CDF) values and fit of squared displacements from a set of trajectories with two diffusion coefficients (*upper*), and the corresponding probability density function which is the derivative of the CDF (*lower*). The simulated values are in grey, the fit is drawn in black. (*C*) A conventional full trajectory MSD curve from pure one-population diffusion (first 500 frames shown). (*D*) A windowed MSD provides an instantaneous diffusion coefficient for all timepoints of a trajectory by performing an MSD analysis only on a segment (the window, as indicated with dashed grey lines in panel *A*) of the trajectory, and sliding this window through the whole trajectory.

Mean squared displacement (MSD)

The most straightforward way to determine the diffusion coefficient is by using the mean squared displacement (MSD) versus time lag curve (1). This provides an estimate of the diffusion coefficient, and also confinement (2), but the method requires that within the complete trajectory there is only one type of homogeneous motion. In short, the MSD is usually defined as the average of all squared distances between points within a certain lag time $\tau = n \cdot \Delta t$, with Δt the time-delay between consecutive frames, and n the interval of frames over which the distance is measured and averaged. For intervals larger than 1 frame, usually all available distances of a given duration $n \cdot \Delta t$ are included, such that the distances are not statistically independent. Yet this way of averaging gives less variance to the average squared displacement value compared to taking only the independent distances (3). For pure Brownian motion, the relation between squared displacements $(\Delta R)^2$ and the diffusion coefficient is a linear relation:

$$\mathrm{MSD}(\tau) = \langle (\Delta R_\tau)^2 \rangle = 4\,D\,\tau + 2\left(\sigma_x{}^2 + \sigma_y{}^2\right) = 4\,D\,\tau + 4\,\sigma_{xy}{}^2 \qquad (1)$$

where σ_{xy} is the standard deviation of the localization inaccuracy in one dimension, which is independent of the time lag. The estimated diffusion coefficient D is found from fitting a line through the points at the different lag times in the MSD curve. We emphasize that it is not straight forward

how to perform the fitting of the MSD curve to obtain diffusion values. A more detailed insight on this is given in the section "Accuracy of MSD methods and CDF fitting to obtain a one population diffusion coefficient" in the Supporting Materials. Moreover, conclusions from MSD curves must always be tested against unconstrained diffusion, as the randomness of normal diffusion may result in apparent anomalous diffusion (4).

A recurring question is which points in the MSD curve can still be considered reliable. Certainly the variance of larger time lags gets increasingly larger, such that the points of larger time lags do not provide any reliable information. In the literature the first 10% points of the curve are often assumed to have not too much variance in their values (5). However, the analytical expression for one population Brownian motion for the variances has been derived (3, 6). Following this expression, Michalet discussed what the optimal number of points is to be taken into the fit for determining the diffusion coefficient (7). The optimal number of points depends on the ratio $\beta = \sigma^2/(D\,\Delta t)$, with σ the standard deviation of the localization inaccuracy. In the limit of no (or relatively small) localization inaccuracy, i.e. for small β, it was shown that the most accurate value for D is obtained by fitting with only the first two points of the MSD curve. This result was already noted earlier (2). However, since we consider two population diffusion systems which have both high and low diffusion constants and correspondingly both low and high β values, we do not readily know the optimal number of points of the MSD curve that should be used in the fit. We have checked how the correctness of the fit depends on the number points of the MSD curve used using simulations (Fig. S2).

Windowed MSD

Typically, the MSD curve is made up from all positions in a trajectory, which cannot resolve local changes in the diffusion coefficient. Windowed MSD tries to give the local or instantaneous diffusion coefficient at each timepoint of a trajectory by performing the MSD analysis on small segments of the trajectory. First an MSD curve is composed for w subsequent positions in a trajectory, and the estimated D value is obtained from the first three points in the curve for this segment. This value is taken as the measure W. Then the MSD curve is made for the next subsequent positions, until the full trajectory has been slid through, and D values have been obtained for each segment, see also Fig. S11D. The use of a moving window makes it possible to detect temporal changes in the mode of motion on the order of the segment length (window size). The resolution is limited by the averaging nature of the method, since reducing the segment length means that the MSD curve is made up from fewer points, therefore increasing the statistical uncertainty of the fitted diffusion coefficient.

Maximum Likelihood Estimation

We have used a likelihood estimation approach here by comparing a window of measured squared displacements, a set of a few single steps $\{(\Delta R)_i\}$, to the expectation value thereof given the distribution function of squared displacements originating from motion with a diffusion constant D. For one step of length ΔR, we use $P((\Delta R)^2|D)$ to express the chance to find a certain squared displacement given Brownian motion with diffusion coefficient D. Since the expectation value of one squared displacement is independent of its predecessors, the chances for a tested D can be multiplied for each squared displacement $(\Delta R)_i{}^2$, hence the likelihood is given by:

$$L(\{(\Delta R)_i\} \mid D) = \prod_{i=1}^{N} \frac{1}{\sqrt{4\pi\left(D\tau + \sigma_{xy}{}^2\right)}} \cdot \exp\left(-\frac{(\Delta R)_i{}^2}{4\left(D\tau + \sigma_{xy}{}^2\right)}\right) \qquad (2)$$

where τ is the time lag, which is 1 frame, and N is the total number of steps in the window. The values for D are taken from the earlier CDF fit. In practice, the localization inaccuracy σ_{xy} must be

determined by other means first. Here we assumed that this value can be precisely obtained, and we used the true value as used in the generation of the trajectories. Here we determine the likelihood of both states, $L_1(\{(\Delta R)_i\} \mid D_1)$ and $L_2(\{(\Delta R)_i\} \mid D_2)$, and if $L_1 > L_2$, the segment is classified as state 1. We could write this as a measure *W* by:

$$W(track, frame) = \frac{L(\{(\Delta R)_i\} \mid D_1)}{L(\{(\Delta R)_i\} \mid D_2)} \tag{3}$$

We have not taken exposure blur into account (8). Note that the MLE can also be used to estimate the value of the diffusion constant itself, by maximizing the expectation value by varying the tested *D* value; the maximum gives the most likely *D* value (9).

Relative confinement

Inspired by the confinement detection method of Simson (10), Meilhac used a slightly altered way to detect confinement (11), which we also use here. The relative confinement is defined by the parameter *L* as:

$$L\left(t_0 + \tfrac{1}{2}\delta t\right) = {}^{\delta t}/_{\text{variance}(s)} \tag{4}$$

$$s = \left| r(t) - r\left(t_0 + \tfrac{1}{2}\delta t\right) \right| \text{ on interval } t = [t_0 .. t_0 + \delta t] \tag{5}$$

An illustration of the distances *s* is given by arrows in Fig. S11A. Here we use the inverse of the value *L* for the motion quantification measure.

Radius of gyration evolution

The use of the radius of gyration has been first proposed by Saxton to measure asymmetry in single molecule trajectories (4), and it was demonstrated by Elliott et al. that it could also be used to detect confinement (12). The gyration radius is a measure of the space that is explored (defined by radius R_g) by the molecule within the segment, hence the radius will have a lower value for slow diffusion than for fast diffusion. Therefore the gyration radius is a local measure of the diffusion of a molecule, and can be used as a differentiation criterion in classification. We note that the expression in reference 12 contains a typographical error, as the radius of gyration is defined as the square root of the non-squared sum of the eigenvalues of the covariance matrix. However we followed Elliot et al. in an alternative measure, also called R_g. This alternative gyration radius R_g is defined as:

$${R_g}^2 = \sqrt{{R_1}^2 + {R_2}^2} \tag{6}$$

where R_1 and R_2 are the eigenvalues of the gyration tensor $\boldsymbol{T}$:

$$\boldsymbol{T} = \begin{pmatrix} \frac{1}{N}\sum_{i=1}^{N}(x_i - \langle x \rangle)^2 & \frac{1}{N}\sum_{i=1}^{N}(x_i - \langle x \rangle)\,(y_i - \langle y \rangle) \\ \frac{1}{N}\sum_{i=1}^{N}(x_i - \langle x \rangle)\,(y_i - \langle y \rangle) & \frac{1}{N}\sum_{i=1}^{N}(y_i - \langle y \rangle)^2 \end{pmatrix} \tag{7}$$

with *i* enumerating all subsequent positions (x_i, y_i) in a segment of length *N*. We will use the value R_g as a motion quantification measure.

Table S1: Motion quantification measures

Method	Quantification measure W
Windowed MSD	*fit of a MSD curve of a segment using first two points in curve*
Confinement	$1/L\left(t_0 + \frac{1}{2}\delta t\right)$
Gyration	R_g
MLE	$\frac{L(\{(\Delta R)_i\} \mid D_1)}{L(\{(\Delta R)_i\} \mid D_2)}$

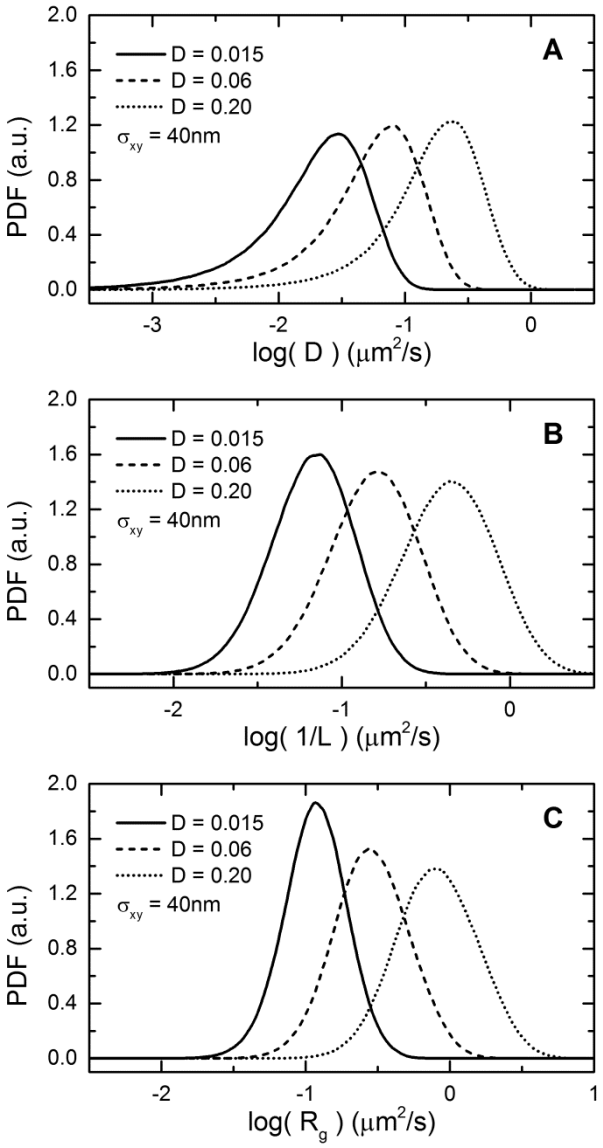

FIGURE S12 Distribution of found quantification measure values for pure one-population diffusion. The histograms of three different diffusion constants are shown, where in all cases we added a localization inaccuracy σ_{xy} of 40 nm to the positions in the simulations. (*A*) Histograms of values found using a windowed MSD. The broadening in the slower diffusion distributions are due to the convolution with the localization inaccuracy. (*B*) Histogram of values found using relative confinement. (*C*) Histogram of values found using gyration.

Live cell experiments methodology

Cell culture

All cell culture materials were obtained from PAA Laboratories (Pasching, Austria) unless stated otherwise. MCF7 cells, a human breast cancer cell line, and plasmid coding for SNAP-EGFR were a gift from Jenny Ibach (Max Planck Institute in Dortmund, Germany). Cells were cultured in Dulbecco's Modified Eagle's medium supplemented with 10% FBS and penicillin/streptomycin at 37°C with 5% CO_2. Before measurements, the cells were transferred to CellView dishes product #627870 (Greiner Bio-one, Alphen aan den Rijn, The Netherlands), grown overnight, transfected with SNAP-EGFR using Effectene (Qiagen, Venlo, The Netherlands), and then starved overnight the day after transfection in medium without FBS. Labeling of the SNAP-EGFR proteins was done by incubating the cells for 1 minute with 400nM of SNAP-Surface 549 (New England BioLabs, Ipswich, MA, USA) in 0.5% BSA. Measurements were performed in PBS buffer with added magnesium and calcium (PAA Laboratories, product H15-001).

Microscopy

Measurements were performed on a microscope with an Olympus PlanApo 100x/1,45 Oil TIRF objective using TIRF illumination. For excitation a 532nm laser (400mW) from Pegasus Shanghai Optical Systems (Pegasus Lasersysteme, Wallenhorst, Germany) was used. All the light filters were obtained from SemRock (Rochester, NY). The infrared light produced by the laser was not sufficiently suppressed, therefore the green laser light passed an FF01-543/22 filter. The excitation and emission is split by an FF494/540/650-Di01 dichroic mirror. The emission light is filtered with an NF03-532/1064E notch filter and an FF01-580/60 bandpass filter. Fluorescence images were acquired using an Andor iXon EM+ DU-897 back illuminated EMCCD with an acquisition time of 9ms and a kinetic cycle time of 38ms (25.8 fps). The microscope stage was heated with a sample heating plate and the objective was heated with a ring heater to 35-37°C.

Tracking

To obtain the trajectories from the raw videos, we used tracking software developed by others (13, 14). The settings used for the cost matrices in this software can be found at the end of the Supporting Materials.

Accuracy of MSD methods and CDF fitting to obtain a one population diffusion coefficient

It might seem, and it is often stated, that the CDF method is more accurate in determining the diffusion coefficient for a one population diffusion system compared to simply averaging the stepsizes as in MSD methods (15), as it considers the whole distribution of stepsizes. In practice however, this is not always correct. Also the number of points from an MSD curve taken into the fit to determine the diffusion coefficient are often based on a "rule of thumb" concept, such as taking the first three or four or the first 10% of the curve. However the accuracy to find the diffusion coefficient can simply be found by simulation and also by calculation (3). We show a simulation approach here to determine the spread of found diffusion coefficients from CDF and MSD methods.

We simulated one-population unconstrained diffusion for 100 trajectories of various lengths, with a relatively small localization error compared to the diffusion coefficient, so for $\beta = \sigma^2/(D\,\Delta t)$ ratio smaller than 1, see (7). We found that, for all lengths of trajectories, a CDF fit with only 1 stepsize is indeed, but only slightly, more accurate compared to the best MSD based fit; the value is of course wrong when not corrected for the added localization inaccuracy to the real diffusion coefficient. In practice this means we have to use the CDF of 2 steps too, and use the difference for CDF 2 steps and CDF 1 step to determine the diffusion coefficient. This 2 steps CDF methods has been described in detail in the methods section. Using this last method however, we found to be less accurate compared to the best MSD based fit where we take only the first two points in the curve (also the 1-steps and 2-steps). Using only the first two points in the MSD curve was the best MSD based fit for this ratio of β. Therefore the CDF was not taken as a method for classification, as the MSD is preferred for one population diffusion therefore. Nevertheless, the CDF method has a known PDF for a distribution with multiple diffusion constants unlike the windowed MSD distribution, so this is still a straight forward method to find the global diffusion constant values and fractions when there are enough datapoints to build a reliable CDF.

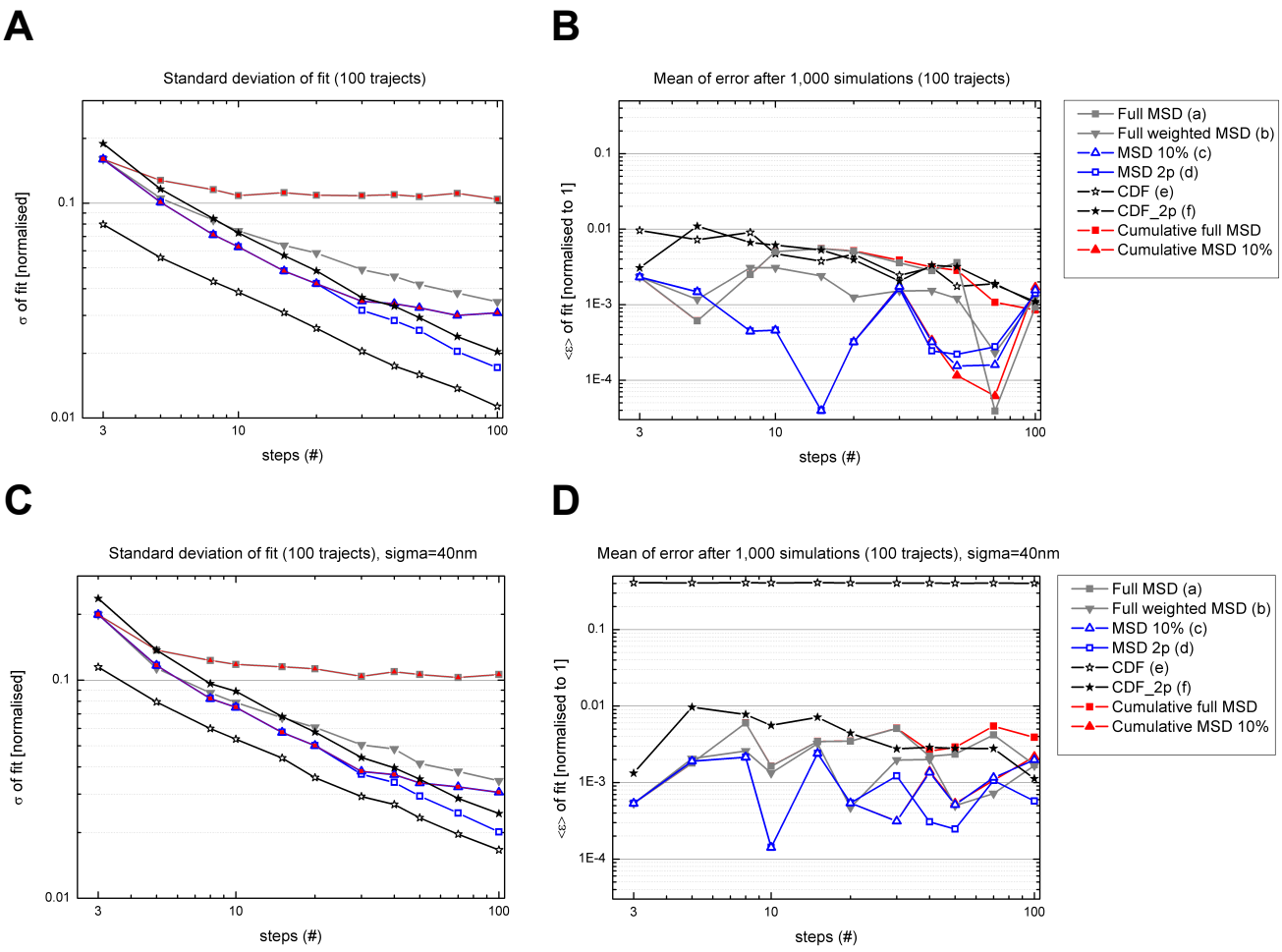

FIGURE S13 Error and standard deviation of MSD methods to obtain a one population diffusion coefficient. For 100 simulated trajectories exhibiting one-population Brownian motion (D=0.1 um^2/s, 25fps) of various lengths (3,5,8,..,100 steps) as plotted on the x-axis, the diffusion value was determined from fitting the MSD curves of all trajectories. We added localization inaccuracy of σ_{xy} = 40nm to the simulated trajectories (*C*,*D*). This fit was done using: the full curve (a), full curve weighted using the variance of each point (b), the first 10% (c), only the first two points (d), and using cumulative distribution function (CDF) fitting of steps (e), and using CDF of one-step and two-step distances (f). We repeated this 1,000 times, and looked at the standard deviation σ *(A,C)*, and the average mismatch <ε> *(B,D)* in the fitted diffusion values. The 1 step CDF method has the lowest standard deviation in the fitted values, but gives the wrong value when there is a localization inaccuracy as in practice. The most accurate way of using the points in the MSD curve, is to only use the first two points of the MSD curve.

Settings file for SPT tracking software

```
Dat.PixelSize = .119;
Dat.TimeStep = 0.03868;
Dat.ch_bin = [1];
Params.verbose = 1;
Params.frames = [];
Params.psf = [0.84034 0.84034];
Params.imMask = [];
Params.wvMask = [];
Params.CCDGain = 63.8298;
Params.CCDOffset = 0;
Params.Intensity = 1.90;
Params.FitBoxSize = [7];
Params.Iterations = 10;
Params.MaxCudaFits = 30000;
Params.MinCRLBSigma = 0.5;
Params.MinPValue = 0.01;
Params.MinPhotons = [10];
Params.ConnectParams.costMatF2Fparams = costMatFrame2FrameSetOptions;
Params.ConnectParams.costMatGCparams = costMatCloseGapsSetOptions;
%%% set parameters for frame 2 frame connections %%%
Params.ConnectParams.costMatF2Fparams.funcName =
'costMatFrame2FrameDensity';
Params.ConnectParams.costMatF2Fparams.density = [];
Params.ConnectParams.costMatF2Fparams.D =
[0.06*Dat.TimeStep/Dat.PixelSize^2 0.06*Dat.TimeStep/Dat.PixelSize^2 ];
Params.ConnectParams.costMatF2Fparams.maxSearchDist = [4 4];
Params.ConnectParams.costMatF2Fparams.kon = 0.1;
Params.ConnectParams.costMatF2Fparams.koff = 0.0001;
Params.ConnectParams.costMatF2Fparams.maxWvSearchDist = [];
Params.ConnectParams.costMatF2Fparams.wvJump = [];
%%% set parameters for gap closing %%%
Params.ConnectParams.costMatGCparams.timeWindow = 10;
Params.ConnectParams.costMatGCparams.funcName = 'costMatCloseGapsDensityM';
Params.ConnectParams.costMatGCparams.density = [];
Params.ConnectParams.costMatGCparams.D = [0.01 0.01];
Params.ConnectParams.costMatGCparams.maxSearchDistPerFrame = [3 3];
Params.ConnectParams.costMatGCparams.maxSearchDist = [10 10];
Params.ConnectParams.costMatGCparams.minTrackLen = 2;
Params.ConnectParams.costMatGCparams.kon = 0.1;
Params.ConnectParams.costMatGCparams.koff = 0.0001;
Params.ConnectParams.costMatGCparams.maxWvSearchDist = [];
Params.ConnectParams.costMatGCparams.wvJump = [];
Params.TrackFunction = 'obj.makeTrack'; % standard two stage tracking call.
```

Supporting References

1. Holtzer, L., and T. Schmidt. 2010. The Tracking of Individual Molecules in Cells and Tissues. In: Bräuchle C, DC Lamb, J Michaelis, editors. Single Particle Tracking and Single Molecule Energy Transfer. WILEY-VCH Verlag GmbH.

2. Wieser, S., and G.J. Schütz. 2008. Tracking single molecules in the live cell plasma membrane-Do's and Don't's. Methods. 46: 131–40.

3. Qian, H., M.P. Sheetz, and E.L. Elson. 1991. Single particle tracking. Analysis of diffusion and flow in two-dimensional systems. Biophys. J. 60: 910–21.

4. Saxton, M.J. 1993. Lateral diffusion in an archipelago. Single-particle diffusion. Biophys. J. 64: 1766–80.

5. De Keijzer, S., A. Sergé, F. van Hemert, P.H.M. Lommerse, G.E.M. Lamers, H.P. Spaink, T. Schmidt, and B.E. Snaar-Jagalska. 2008. A spatially restricted increase in receptor mobility is involved in directional sensing during Dictyostelium discoideum chemotaxis. J. Cell Sci. 121: 1750–7.

6. Saxton, M.J. 1997. Single-particle tracking: the distribution of diffusion coefficients. Biophys. J. 72: 1744–53.

7. Michalet, X. 2010. Mean square displacement analysis of single-particle trajectories with localization error: Brownian motion in an isotropic medium. Phys. Rev. E. 82: 041914.

8. Berglund, A. 2010. Statistics of camera-based single-particle tracking. Phys. Rev. E. 82: 011917.

9. Montiel, D., H. Cang, and H. Yang. 2006. Quantitative characterization of changes in dynamical behavior for single-particle tracking studies. J. Phys. Chem. B. 110: 19763–70.

10. Simson, R., E.D. Sheets, and K. Jacobson. 1995. Detection of temporary lateral confinement of membrane proteins using single-particle tracking analysis. Biophys. J. 69: 989–93.

11. Meilhac, N., L. Le Guyader, L. Salomé, and N. Destainville. 2006. Detection of confinement and jumps in single-molecule membrane trajectories. Phys. Rev. E. 73: 011915.

12. Elliott, L.C.C., M. Barhoum, J.M. Harris, and P.W. Bohn. 2011. Trajectory analysis of single molecules exhibiting non-brownian motion. Phys. Chem. Chem. Phys. 13: 4326–34.

13. Low-Nam, S.T., K. a Lidke, P.J. Cutler, R.C. Roovers, P.M.P. van Bergen En Henegouwen, B.S. Wilson, and D.S. Lidke. 2011. ErbB1 dimerization is promoted by domain co-confinement and stabilized by ligand binding. Nat. Struct. Mol. Biol. 18: 1244–1249.

14. Smith, C.S., N. Joseph, B. Rieger, and K.A. Lidke. 2010. Fast, single-molecule localization that achieves theoretically minimum uncertainty. Nat. Methods. 7: 373–5.

15. Brauchle, C., D.C. Lamb, and J. Michaelis. Single Particle Tracking and Single Molecule Energy Transfer. Weinheim: WILEY-VCH Verlag GmbH.